# Redox regulation of ryanodine receptor/$Ca^{2+}$ release channels by NOX enzymes in hypertrophy and heart failure

Dissertation

for the award of the degree

“Doctor rerum naturalium”

of the Georg-August-Universität Göttingen

within the doctoral program “Molecular Medicine”
of the Georg-August University School of Science (GAUSS)

submitted by
Dennis Uhlenkamp

born in Ostercappeln, Germany

Göttingen, 2021

**Thesis Committee**

Prof. Dr. Stephan E. Lehnart (Supervisor)
Department for Cardiology and Pneumology, University Medical Center, Göttingen

Prof. Dr. Dörthe M. Katschinski
Institute of Cardiovascular Physiology, University Medical Center, Göttingen

Prof. Dr. Tobias Moser
Institute for Auditory Neuroscience & InnerEarLab, University Medical Center, Göttingen

**Members of the Examination Board**

Referee:
Prof. Dr. Stephan E. Lehnart (Supervisor)
Department for Cardiology and Pneumology, University Medical Center, Göttingen

2nd Referee:
Prof. Dr. Dörthe M. Katschinski
Institute of Cardiovascular Physiology, University Medical Center, Göttingen

**Further members of the Examination Board**

Prof. Dr. Ralph Kehlenbach
Department of Molecular Biology, University Medical Center, Göttingen

PD Dr. Laura Zelarayán-Behrend
Institute of Pharmacology and Toxicology, University Medical Center, Göttingen

Prof. Dr. Thomas Meyer
Department for Psychosomatic Medicine and Psychotherapy, Molecular Psychocardiology, University Medical Center, Göttingen

Date of oral examination: 20.01.2021

*To my family*

# Table of contents

## List of Publications

Hannah M Campbell, Ann P Quick, Issam Abu-Taha, David Y Chiang, Carlos F Kramm, Tarah A Word, Sören Brandenburg, Mohit Hulsurkar, Katherina M Alsina, Hui-Bin Liu, Brian Martin, Dennis Uhlenkamp, Oliver M Moore, Satadru K Lahiri, Eleonora Corradini, Markus Kamler, Albert J R Heck, Stephan E Lehnart, Dobromir Dobrev, Xander H T Wehrens, Loss of SPEG Inhibitory Phosphorylation of Ryanodine Receptor Type-2 Promotes Atrial Fibrillation. Circulation. 2020 Sep 22;142(12):1159-1172.
doi: 10.1161/CIRCULATIONAHA.120.045791.

In preparation:
Sören Brandenburg, Jan Pawlowitz; Vanessa Steckmeister; Hariharan Subramanian; Dennis Uhlenkamp; Marina Scardigli; Mufassra Mushtaq; Saskia I. Amlaz; Tobias Kohl; Jörg W. Wegener; Demetrios A. Arvanitis; Despina Sanoudou; Leonardo Sacconi; Gerd Hasenfuß; Niels Voigt; Viacheslav O. Nikolaev; Stephan E. Lehnart. A junctional cAMP compartment regulates rapid $Ca^{2+}$ signaling in atrial myocytes

# List of figures

# Abbreviations

| | |
|---|---|
| °C | degree Celsius |
| aa | Amino acid |
| Ad5 | Adenovirus serotype 5 |
| BCS | Bovine calf serum |
| cDNA | Complementary deoxynucleic acid |
| CMV | cytomegalovirus |
| $CO_2$ | carbon dioxide |
| CRU | Calcium release unit |
| DHPR | Dihydropyridine receptor |
| DMEM | Dulbeccos modified eagle medium |
| DNA | Deoxynucleid acid |
| ECC | Excitation-contraction coupling |
| EDTA | Ethyldiamintetraacetate |
| eGFP | enhanced green fluorescence protein |
| ER | Endoplasmic Reticulum |
| FBS | fetal bovine serum |
| Fwd | forward |
| HEK | human embryonic kidney cells |
| IRES | Internal ribosomal entry site |
| KO | Knockout |
| MOI | Multiplicity of infection |
| mRNA | Messenger ribonucleic acid |
| MS | Mass spectrometry |
| $N_2$ | nitrogen |
| NaCl | sodium chloride |
| NADPH | Nicotinamide adenine dinucleotide phosphate |
| NOX | NADPH-dependent oxidase |
| $O_2$ | dioxide |
| PBS | Phosphate buffer saline |
| PCR | Polymerase chain reaction |
| Pen/Strep | penicillin/streptomycin |
| PFA | Paraformaldehyde |
| Rev | reverse |
| RT | room temperature |
| RyR2 | Ryanodine receptor type 2 |

| | |
|---|---|
| hRyR2 | Human Ryanodine receptor type 2 |
| sec | second |
| SERCA | Sarcoendoplasmic reticulum Calcium ATPase |
| SR | Sarcoplasmic reticulum |
| STED | Stimulated Emission Depletion |
| TAC | transvers aortic constriction |
| Tg | transgenic |
| VCM | Ventricular cardiomyocytes |

## Acknowledgement

First of all, I would like to express my gratitude to Prof. Dr. Stephan E. Lehnart for providing the opportunity to prepare my Ph.D. in his group. Thank you for the continuous support and the supervision of this doctoral thesis.

Additionally, I would like to thank Prof. Dr. Dörthe Katschinski and Prof. Dr. Tobias Moser for being members of my thesis advisory committee. I greatly appreciated the valuable input, and the constructive discussions during my PhD time. I would like to thank especially Prof. Dr. Dörthe Katschinski for evaluating this thesis.
My thanks extend to PD Dr. Laura Zelarayan-Behrend, Prof. Dr. Ralph Kehlenbach and Prof. Dr. Thomas Meyer for joining my extended thesis examination board.

I want to thank Prof. Ajay Shah and his lab, especially Dr. Celio Santos, at the King's College London, for the opportunity to visit your lab within the IRTG1816 project and to gain valuable feedback and experiences.

Moreover, I would like to thank all current and past members of the AG Lehnart. Thanks for creating a productive and fun work atmosphere, for the feedback when sharing experiments and plans. Many thanks to Brigitte, Birgit, and Christiane for your support and technical assistance in and outside the lab.

I simply cannot express how grateful I am to Jan, Daniel, Jonas, and Luca. It was only through your support, your feedback, and the always sympathetic ears that I was able to take the final steps of this journey.

A special shout-out goes to Julien, Iris, Kathrin, Kevin, Steffi, Paula, Luca and Johanna. Ten years ago, we started this crazy journey together. What may have begun as a Zweckgemeinschaft quickly became the best thing about Greifswald, and I am extremely grateful that we still keep in touch.

Last but most definitely not least I want to thank my family for their constant and loving support and for a home that I can always and happily return to.

## Abstract

Cardiac function is characterized by a rhythmic sequence of contraction and relaxation of cardiomyocytes driven by tightly controlled intracellular calcium release events. The cardiac ryanodine receptor type 2 calcium release channel, RyR2, provides a key function for this cyclic $Ca^{2+}$ release and thus cardiomyocyte contraction. Posttranslational RyR2 modifications through redox-sensitive cysteine residues were shown to increase channel activity, which may lead to $Ca^{2+}$ leak from the sarcoendoplasmic reticulum. This has been associated with pathological conditions such as heart failure. However, precise molecular mechanisms of redox-mediated RyR2 (dys)regulation remain to be identified. The aim of this thesis was to characterize the redox-based regulation of RyR2 $Ca^{2+}$ release channels by the cardiac isoforms of the ROS-generating NADPH-dependent oxidases NOX2 and NOX4.

To study NOX-dependent redox modifications of RyR2 channels, cardiac NOX enzymes and RyR2 were expressed in HEK293A cells. Spontaneous changes in cytosolic $Ca^{2+}$ levels were measured by live-cell epifluorescence microscopy. RyR2-overexpressing HEK293A cells showed self-regenerative $Ca^{2+}$ waves, which were inhibited by the specific $Ca^{2+}$ channel inhibitor ryanodine. Importantly, short-time incubation with hydrogen peroxide ($H_2O_2$) caused a significant increase in $Ca^{2+}$ waves frequency of 49.95 s ± 2.5 (ctrl) vs. 41.23 s ± 1.3 (1 mM $H_2O_2$), (n=8, $p<0.01$ (unpaired t-test)). To validate NOX-dependent $H_2O_2$ production in HEK293A cells, $H_2O_2$ was directly monitored by co-expression of the genetically encoded HyPer-3 biosensor. Expression of the cardiac NOX2 and NOX4 both resulted in significantly increased $H_2O_2$ levels [HyPer-3 ratio: 0.596 ± 0.014 (ctrl) vs. 0.71 ± 0.025 (NOX2) vs. 0.67 ± 0.024 (NOX4), n=134, $p<0.05$ (ANOVA)].

To investigate the thus far unclear subcellular localization of NOX4 and its spatial relation to RyR2 channel clusters in their native cardiomyocyte environment, an adenoviral expression construct was designed to induce expression of NOX4 in isolated primary mouse ventricular cardiomyocytes. STED nanoscopy of NOX4-transduced cardiomyocytes (Ad5.NOX4) revealed a NOX4 localization at the sarcoplasmic reticulum bringing it in close proximity to RyR2 clusters. A co-localization analysis demonstrated a significantly increased spatial overlap between RyR2 and NOX4 clusters in Ad5.NOX4-transduced cardiomyocytes compared to control [67.5% ± 2.1 (Ad5-NOX4) vs. 22.9% ± 12.7 (Ad5-eGFP), n≥3, $p<0.01$ (t-test)]. Further, the area of NOX4 clusters overlapping with RyR2 clusters was significantly larger compared to non-overlapping NOX4 clusters, indicating a regulatory complex formation [(0.0177 µm2 ± 0.002 (overlapping clusters) vs. 0.008 µm2 ± 0.001 (independent clusters) n≥3, $p<0.01$ (t-test)]. By performing co-immunoprecipitation assays, a direct protein-protein interaction of NOX4 and RyR2 was revealed, further emphasizing a potentially regulatory NOX4/RyR2 complex in virally transduced cardiomyocytes.

Since a direct protein-protein interaction of NOX4 and RyR2 could be demonstrated, specific cysteine residues of RyR2 serving as target for a NOX-dependent oxidation were further investigated. To identify these cysteine residues, a differential alkylation assay was established allowing distinct labeling of oxidized cysteines for a subsequent data-independent mass spectrometry analysis.

The HEK293A cell model and the results presented here serve as an experimental framework for simultaneous monitoring of $Ca^{2+}$ waves and $H_2O_2$ production through combinatory RyR2/NOX2- and RyR2/NOX4-transfections together with HyPer-3 by multi-color epifluorescence microscopy. Moreover, STED nanoscopy revealed a SR localization of NOX4 and a close association with RyR2 channels in cardiomyocytes. This association was further consolidated by co-immunoprecipitation and demonstrated to be a direct protein interaction.

In summary, this thesis provides novel insights into the interaction between the RyR2 $Ca^{2+}$ channel and NOX enzymes and introduces the groundwork for future comprehensive studies of the hypothesized regulatory impact of NOX-generated ROS on RyR2 channel function in cardiomyocytes.

# 1. Introduction

Heart function is characterized by rhythmic contractions of the cardiac muscle tissue in order to pump blood through the cardiovascular system of an organism [1]. This contraction is facilitated by cardiomyocytes, heart-specific muscle cells. Cardiomyocytes form a functional syncytium to ensure coordinated contraction and thus sufficient pumping function [2]. The regulation of intracellular calcium ion ($Ca^{2+}$) concentrations is a crucial element in the coordination of cardiomyocyte contraction [3]. In a process termed excitation-contraction coupling (EC-coupling), $Ca^{2+}$ is directly responsible for transmitting the electrical stimulus of an action potential into the mechanical shortening of sarcomeric myofilaments and thus cardiomyocyte contraction [4]. Initially, voltage-gated L-type $Ca^{2+}$ channels (dihydropyridine receptors (DHPRs)) are activated by the action potential and allow a relatively small influx of extracellular $Ca^{2+}$ into the myocyte [5]. This results in a locally increased $Ca^{2+}$ concentration in the dyadic cleft, a subcellular compartment characterized by a close contact of the sarcolemma and the sarcoplasmic reticulum (SR) membrane [6]. Here, the initial calcium influx via L-type $Ca^{2+}$ channels activates a much larger intracellular $Ca^{2+}$ release from the SR through type 2 ryanodine receptor channels (RyR2), known as calcium induced $Ca^{2+}$ release (CICR) [7]. This global increase in $Ca^{2+}$ concentration activates myofilament contraction by binding of $Ca^{2+}$ to troponin C (TnC), the $Ca^{2+}$-binding component of the thin myofilament [8]. In order to terminate cardiac muscle contraction and initiate relaxation, DHPRs and RyR2 are inactivated and $Ca^{2+}$ is removed from the cytosol by sarcolemmal $Ca^{2+}$-ATPases (PMCA) and $Na^{2+}/Ca^{2+}$ antiporters (NCX) [9,10]. However, the vast majority of $Ca^{2+}$ removal is facilitated by the sarco/endoplasmic reticulum $Ca^{2+}$-ATPase 2a (SERCA2a), located in the SR membrane [11]. Taken together, this highly orchestrated sequence of $Ca^{2+}$ influx and efflux is crucial and fundamental for proper cardiomyocyte function.

## 1.1. Type 2 ryanodine receptor/$Ca^{2+}$ release channel

Dysregulation of calcium handling in cardiomyocytes is often the cause or accompanying symptom of pathophysiological conditions such as heart failure (HF), arrhythmias and hypertrophic cardiomyopathy (HCM). These conditions are characterized by an increase in diastolic $Ca^{2+}$ concentration, attributed either to an impaired $Ca^{2+}$ reuptake into the SR due to decreased SERCA2a activity or to $Ca^{2+}$ leak from the SR as a result of RyR2 channel dysregulation [3].

Type 2 ryanodine receptor/$Ca^{2+}$ release channels are an important part of the calcium-handling machinery in cardiomyocytes. There are three isoforms of RyR (RyR1-3) sharing around 65 % of

sequence homology [12]. While RyR1 is the predominant isoform found in skeletal muscle cells and RyR3 is expressed in skeletal muscles and in the brain, RyR2 is predominantly expressed in the heart [13,14]. RyR2 is a large protein with a molecular mass of ca. 550 kilo Dalton (kDa), forming even larger homotetramers (> 2 MDa) to facilitate their $Ca^{2+}$ channel function [15]. RyR2 is localized at the junctional sarcoplasmic reticulum membrane (jSR), where it is organized in clusters of about 10 RyR2 channels [16,17]. Together with DHPRs, localized at regular invaginations of the sarcolemma (T-tubules), it forms calcium release units (CRUs) [18]. Structurally, there are two major regions of the RyR2 protein. The C-terminal transmembrane region is responsible for the formation of the ion-conducting pore [19]. The larger part of the protein (~ 80%) resides in the cytosol and is the target for numerous RyR2-regulating proteins, the most important of which are discussed in more detail below [12 20].

As RyR2 channel activity is directly linked to cardiomyocyte function, its regulation is tightly controlled. This ensures a constant adaptation to changing physiological demands of the cardiovascular system, e.g., exercise or rest. A major way for this adaptation of RyR2 channel activity is facilitated by phosphorylation. Stimulation of β1-adrenergic receptors by catecholamines (e.g., adrenaline, noradrenaline) in response to exercise or other stresses (fight-or-flight response) results in the activation of protein kinase A (PKA). In addition to other proteins involved in $Ca^{2+}$-handling, PKA phosphorylates RyR2 at the serine residue 2808 (Ser2808), which is reported to increase RyR2 channel activity [21]. Besides PKA, RyR2 is additionally phosphorylated by the $Ca^{2+}$/calmodulin-dependent kinase II (CaMKII) at Ser2814 [22]. While Ser2808 is uniquely phosphorylated by protein kinase A (PKA), Ser2814 is reported to be exclusively CaMKII-phosphorylated [21–23]. Protein phosphatases 1 (PP1) and 2A (PP2A) are associated with RyR2 to facilitate dephosphorylation [24]. Dysregulation of RyR2 phosphorylation as a result of chronically increased activation of PKA and CaMKII has been implicated in pathophysiological conditions including heart failure and arrhythmias [23].

Direct protein-protein interactions are another way of modulating RyR2 channel activity. The FK-binding protein 12.6 (FKBP12.6) binds to a region in the cytosolic domain of RyR2 [25]. This interaction stabilizes RyR2 and allows a tight control of the closed and open state of the RyR2 channel [26]. Abrogation of this interaction, for example by acute PKA hyperphosphorylation of Ser2808 or by RyR2 mutations, increases the open probability of RyR2 and presents a potential link to arrhythmias such as catecholaminergic polymorphic ventricular tachycardia (CPVT) [27,28]. CPVT is characterized as an exercise or stress induced condition of ventricular arrhythmias and tachycardia in an otherwise healthy heart, often resulting in sudden cardiac death [29].

Calmodulin (CaM), a $Ca^{2+}$-binding protein, regulates RyR2 channel activity by direct interaction with its cytosolic domain. It binds to RyR2 in both its $Ca^{2+}$-bound and $Ca^{2+}$-free form and modulates $Ca^{2+}$ release from the SR by lowering the calcium sensitivity of RyR2 [30,31]. Reduced

interaction of CaM and RyR2, resulting in spontaneous and local $Ca^{2+}$ release-triggering arrhythmias, is reported in a CPVT mouse model [32].

Besides regulation via the cytosolic domain of RyR2, proteins in the SR lumen have also been described to regulate RyR2 channel function. Calsequestrin 2 (Casq2) is a cardiac $Ca^{2+}$-binding protein important for $Ca^{2+}$ storage in the SR lumen [33]. It is described to regulate RyR2 depending on its $Ca^{2+}$-binding state and hence $Ca^{2+}$ load in the SR. Junctin and triadin, two SR-membrane proteins, are additionally required for the Casq2/RyR2 interaction, as they form a complex with Casq2 and RyR2 at the junctional SR [34].

In addition to RyR2 channel activity regulation by the described mechanisms, there is increasing evidence of a redox-dependent regulation of RyR2, including oxidation, glutathionylation and S-nitrosylation [35–37]. As this redox modification of RyR2 is a focus of this thesis, basic principles of redox signaling are described below.

## 1.2. Redox signaling

The concept of redox signaling has evolved profoundly over the last decades. Redox signaling, which describes the orchestrated process of specific reduction and oxidation events, has initially been attributed to a global cellular balance of pro- and antioxidative molecules. Conditions in which this global balance is disturbed were held responsible for causing uncontrolled and unspecific redox-dependent modifications. A more recent understanding of redox-dependent signaling, however, highlights controlled, specific and reversible redox events as crucially important [38,39].

This modern concept of redox signaling involves protein thiol groups of cysteine residues as a major target of redox-dependent modifications (Figure 1) [40]. Cysteine thiols are susceptible to reversible oxidation yielding a sulfenic acid [41]. This form is highly reactive and can form inter -and intramolecular disulfide bonds with other protein thiol groups or with the thiol group of glutathione, a small cysteine-containing peptide, known as glutathionylation [42]. Further oxidation of the sulfenic acid results in the formation of sulfinic and eventually sulfonic acid, which are both considered to be irreversible [40]. Nitric oxide (NO) or S-Nitrosoglutathione (GSNO) are also able to redox-modify cysteine residues resulting in S-nitrosylation [43].

In order for cysteine thiols to be susceptible to these modifications, they need to meet certain criteria [44]. Surface exposure of cysteines is a prerequisite to be targeted by redox signaling. Furthermore, the reactivity of a cysteine thiol group is directly linked to its immediate environment within the protein. Neighboring basic or positively charged amino acids (e.g. lysine, arginine) are able to lower the specific $pK_a$ value of a thiol from about eight to six, rendering the thiol group significantly more reactive at physiological pH values [43,45,46].

Reactive oxygen species (ROS) and reactive nitrogen species (RNS), specifically hydrogen peroxide ($H_2O_2$) and nitric oxide (NO), are the major cellular compounds causing the redox modifications described above [47,48]. Endogenous $H_2O_2$ is produced by the enzymatic conversion of superoxide ($O_2^-$) to $O_2$ and $H_2O_2$ [49]. Other major enzymatic sources of $H_2O_2$ are members of the nicotinamide adenine dinucleotide phosphate (NADPH) oxidase (NOX) family, xanthine oxidases (XO) or the mitochondrial complexes I and III of the electron transport chain [50–52]. Nitric oxide is enzymatically synthesized by one of three eukaryotic NO-synthase isoforms [53,54].

While redox-dependent cysteine thiol modifications are crucially important for numerous physiological signaling pathways, an excessive and uncontrolled occurrence of protein oxidation is also involved in the development or progression of pathophysiological conditions. This excess of oxidation events due to increased levels of ROS or RNS is known as oxidative stress [55]. To counterbalance uncontrolled ROS or RNS production, the cell harnesses a vast intrinsic antioxidant system. Superoxide dismutases (SOD) and catalases detoxify superoxide and

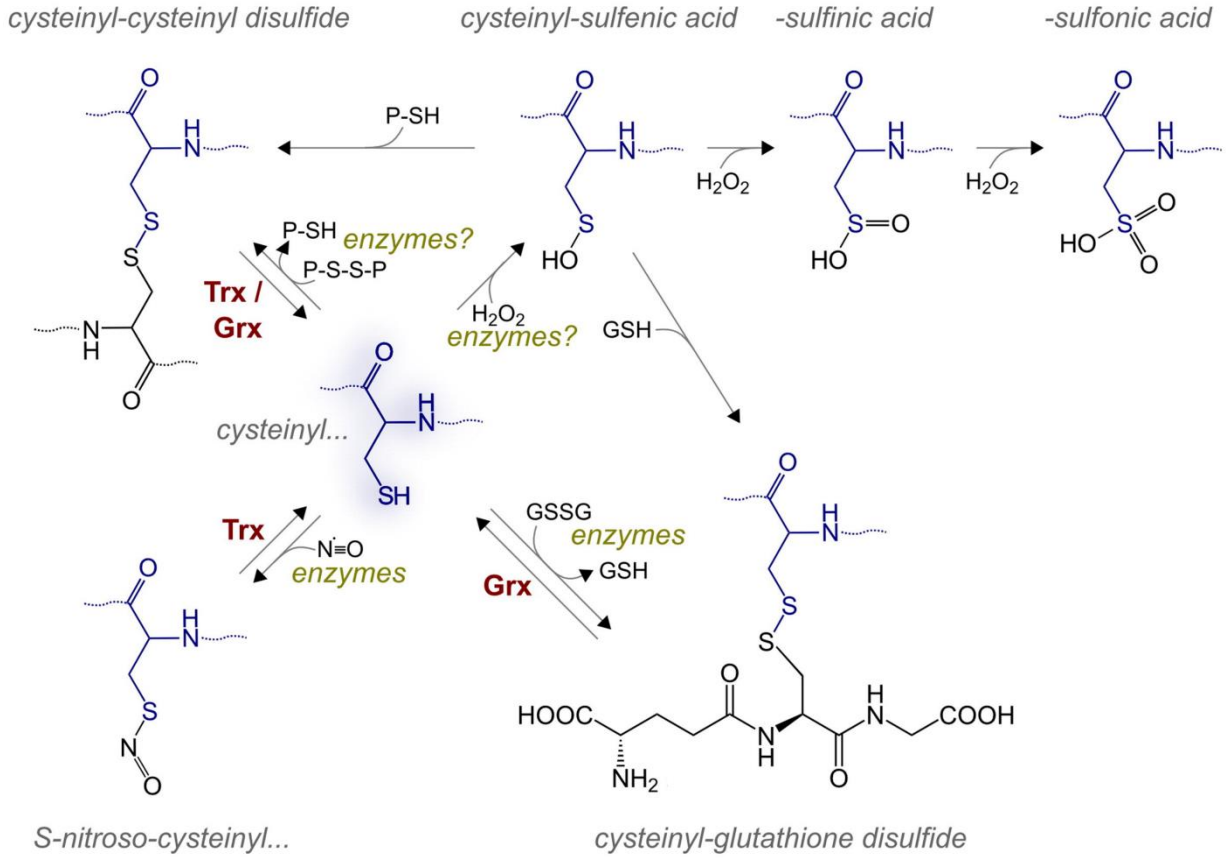


***Figure 1: Redox modifications of cysteine residues.***

*Cysteine residues can be oxidized by $H_2O_2$, e.g., resulting in the formation of a sulfenic acid. This sulfenic acid can either react with another cysteine residue to form a disulfide bond, or it can be further oxidized to sulfinic and sulfonic acid. The inter- or intramolecular disulfide can be reduced by Thioredoxins (Trxs) or Glutaredoxins (Grxs). Additionally, cysteine residues can react with glutathione disulfide (GSSG), resulting in glutathionylation. Nitric oxide (NO) or S-Nitrosoglutathione (GSNO) are able to redox-modify cysteine residues in a process called S-nitrosylation.*

*Scheme adapted from Gellert et al., BBA, 2015.*

hydrogen peroxide [49]. Additionally, members of the glutaredoxin (Grx), thioredoxin (Trx) or peroxiredoxin (Prx) family, ubiquitously expressed in many cell types, are frequently involved in the specific reduction of oxidative modifications [56–59].

Taken together, redox signaling describes a complex and highly regulated system of specific and reversible oxidation and reduction events.

## 1.3. Redox modification of RyR2 channel activity

As redox modifications are frequently involved in cell signaling, it has been shown that RyR2 channel activity is also regulated by redox-dependent modification. Being a very large protein, RyR2 features 90 cysteine residues in its amino acid sequence, of which only a subset of 21 are present in the free thiol state [37,60]. Studies on the redox-dependent regulation of the skeletal muscle isoform RyR1 have identified certain cysteine residues as “hyperreactive”, i.e. highly susceptible, to redox modifications [61,62]. The amino acid sequences that encompass cysteines in RyR1 and RyR2 show a high degree of homology, suggesting that reactive cysteines found in RyR1 are equivalently present in RyR2 [63].

It has been described that RyR2 shows a low basal level of S-nitrosylation [37]. This S-nitrosylation, mainly attributed to be caused by cardiac NO-synthases, has been associated with an increase in RyR2 channel activity [64]. An excess of RyR2 nitrosylation, however, results in channel inhibition [65]. Physiologically, the basal level of RyR2 S-nitrosylation might be beneficial for proper channel activity, as hyponitrosylated RyR2 is more prone to irreversible oxidation of cysteine thiols and thus disturbed channel function, expressed as diastolic $Ca^{2+}$ leak [66,67].

A similar protective role is described for S-glutathionylation of RyR2 [68]. Studies have shown that NOX-dependent S-glutathionylation of RyR2 was increased after exercise or tachycardia, which are conditions associated with an increase in ROS production [69]. The formation of a mixed disulfide of GSH and RyR2 has also been described to act as a potential intermediate step in inter- or intramolecular disulfide bond formation [70].

Increased RyR2 oxidation is additionally involved as a crucial factor in the pathogenesis of heart failure. Elevated levels of RyR2 oxidation in the failing heart have been linked to enhanced RyR2 channel activation resulting in diastolic $Ca^{2+}$ leak and thus decreased $Ca^{2+}$ concentrations in the SR [71].

While RyR2 has been identified as a major target for redox dependent modifications in healthy and pathophysiological conditions, the exact mechanisms and regulatory consequences of these processes are not fully understood. In the search for enzymes involved in cardiac redox signaling, NOX enzymes have been associated with cardiac ROS production as well as redox regulation of RyR2 and will be focused on in this thesis.

## 1.4. NADPH-dependent oxidases

It has long been believed that ROS production was a mere byproduct of other biological processes. While this applies, for example, to processes of the mitochondrial electron transport chain, the identification of a family of enzymes that specifically generates ROS has challenged this view. The family of NADPH-dependent oxidases comprises seven proteins, NOX1-5 and DUOX1-2, which form membrane-bound enzyme complexes with other regulatory proteins [72]. NOX2, or gp91$^{phox}$, was the first isoform that had been identified in phagocytes, where it is involved in host defense mechanisms against pathogens by generating a respiratory burst of ROS [73]. It has since been extensively studied and is regarded as the prototypical NOX enzyme, featuring important structural properties, which are conserved in all members of the NOX family (Figure 2).

NOX enzymes are transmembrane proteins with six transmembrane domains. To exert their function as oxidoreductases, they contain two heme groups, coordinated by highly conserved histidine residues in the transmembrane domain III and V, respectively, and C-terminal binding sites for flavin adenine dinucleotide (FAD) and NADPH [74,75]. Functionally, NOX enzymes can be

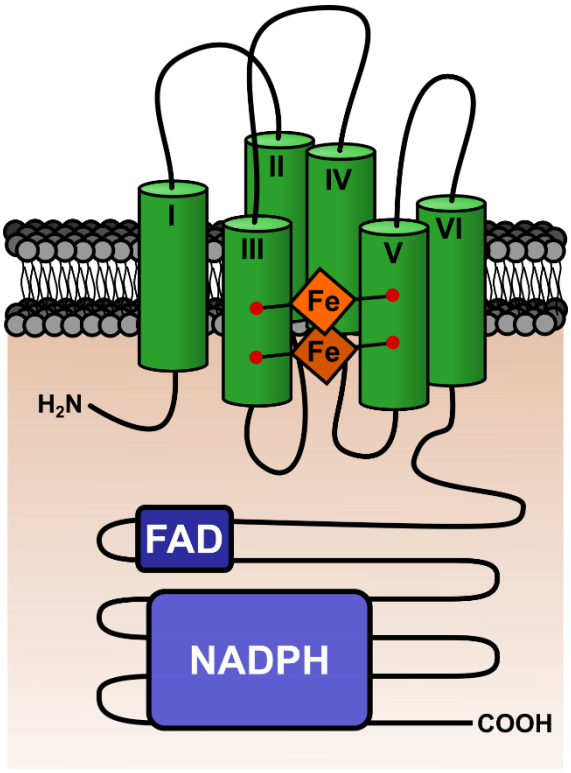


***Figure 2: Conserved structural properties of NOX family enzymes.***
*NOX enzymes are transmembrane proteins featuring six transmembrane domains (I – VI). Four highly conserved histidines in transmembrane domain III and V coordinate two iron-containing heme groups. Together with a C-terminal FAD and NADPH binding region, they are responsible for the transport of electrons from NADPH to molecular $O_2$. Adapted from Bedard and Krause, PhysRev, 2007.*

described as an electron transport chain across a biological membrane [72]. Upon binding of NADPH to its cytosolic binding site, two electrons are transferred to the non-covalently bound FAD, yielding reduced $FADH_2$. One electron is then passed to the first and subsequently to the second heme group. As this transfer is energetically unfavorable, it only takes place if molecular oxygen is present to receive the electron from the second heme group, thus forming superoxide ($O_2^-$). These steps are then repeated to pass the second electron from the semi-reduced FADH to another oxygen molecule [76]. In principle, this transfer of electrons from the donor NADPH to the acceptor oxygen is rate-limited by the initial electron transfer from NADPH to FAD [76]. In the cell biological context, however, NOX enzyme complex activity is controlled by the interaction of NOX with regulatory cytosolic subunits.

### 1.4.1. NADPH oxidase complex formation and regulation

Detailed studies of the biochemical and biological properties of NOX2 have provided insight into general NOX enzyme complex formation and regulation.

NOX2 forms a heterodimer with the transmembrane protein p22phox [77]. This heterodimer formation is important for protein stability, as it prevents the degradation of the NOX2 enzyme [78]. Activation of the enzyme complex requires binding of further cytosolic proteins to the NOX2/p22phox dimer. Phosphorylation of p47phox enables the interaction of its tandem

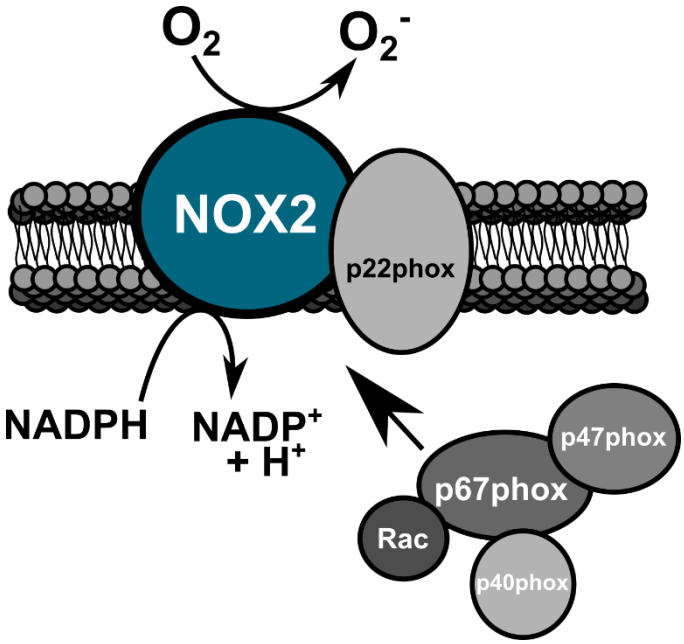


***Figure 3: NOX2 complex formation.***

*The enzymatic subunit of the NOX2 complex constitutively interacts with p22phox. Complex formation and activation require interaction of p47phox, p40phox, p67phox and Rac with the NOX2/p22phox dimer. Upon activation, electrons are transferred from NADPH to molecular oxygen, yielding superoxide. Adapted from Sirker et al., Basic Res Cardiol, 2011.*

Src-homolgy (SH) domains with the proline-rich region (PRR) of p22phox [79]. As p47phox orchestrates binding of additional subunits to the NOX2 complex, it is referred to as the "organizer subunit" [72]. The interaction of p67phox with the NOX2 subunit is prerequisite for the activation of the enzymatic activity of NOX2 [80]. Finally, the small GTPase Rac associates to the complex by binding to both NOX2 and p67phox [81,82].

Other isoforms of the NOX oxidase family differ from mechanisms of NOX2 complex formation and activation.

NOX1 and NOX3 were the first identified homologs of NOX2, sharing approximately 60 % of amino acid identity with NOX2 [83,84]. Predominantly expressed in colon epithelium, NOX1 is also present in vascular smooth muscle cells and endothelial cells [85–87]. NOX3 is highly abundant in specific parts of the inner ear, including the cochlea and vestibular sensory epithelia [84]. While NOX1 and NOX3 both interact with p22phox, functional NOX complex formation and activation includes NOXO1, a p47phox homolog, and NOXA1, a p67phox homolog [88]. However, *in-vitro* recombination studies have demonstrated that NOX1 and NOX3 are also activated by p47phox and p67phox [89,90].

NOX4, first discovered as an NADPH oxidase isoform highly expressed in the kidney, is more distinct from NOX1-3 in terms of amino acid homology, as it only shares around 39 % identity with NOX2 [72,91]. The gene for NOX4 gives rise to four additional splice variants (NOX4B-E) [92]. NOX4 also differs from NOX1-3 in terms of its activation, since active NOX4 complex formation only requires p22phox and no further cytosolic subunits (Figure 4) [93]. In this NOX4/p22phox complex, p22phox not only stabilizes NOX4 but is also important for NOX4-dependent ROS

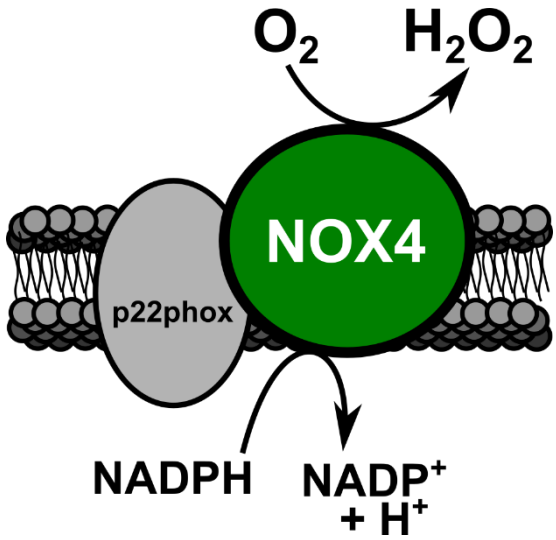


***Figure 4: NOX4 complex.***

*Active NOX4/p22phox complex formation does not require interaction with further cytosolic subunits. NOX4 is constitutively active and generates preferably $H_2O_2$. Adapted from Sirker et al., Basic Res Cardiol, 2011.*

generation [94]. Since NOX4 enzyme activity is not regulated by cytosolic subunits, it is considered constitutively active with its regulation being directly linked to protein abundancy and NOX4/p22phox complex formation [95]. Importantly, NOX4 is described to preferably produce $H_2O_2$ instead of $O_2^-$. Studies revealed the E-loop of NOX4, which connects transmembrane domain V and VI, to be involved in spontaneous dismutation of NOX4-generated $O_2^-$ to $H_2O_2$ [96].

The interaction of the enzymatic NOX subunit with p22phox is not present in all isoforms. NOX5, which is expressed in a variety of tissues such as testis, spleen and lymph nodes, does not require complex formation with p22phox for its enzymatic activity. Instead, It features an extended cytosolic N-terminus that contains three $Ca^{2+}$-binding EF hand motifs important for regulation of its activity [97]. DUOX1 and DUOX2, oxidases identified in the thyroid gland, also contain these $Ca^{2+}$-binding domains and are equipped with an additional N-terminal transmembrane domain [98]. Similar to NOX5, interaction with p22phox is not required and DUOX1/2 activity is regulated by $Ca^{2+}$-binding [99].

While many isoforms of the NADPH oxidase family have been identified to be expressed in cells of the cardiovascular system, including vascular smooth muscle cells, endothelial cells or cardiac fibroblast, this work focuses on NOX2 and NOX4, the only isoforms expressed in cardiomyocytes.

## 1.5. Cardiac NOX oxidases: NOX2 and NOX4

NOX2 and NOX4 are the cardiac NADPH oxidase isoforms expressed in cardiomyocytes [100,101]. As indicated above, NOX2 and NOX4 show distinct characteristics, which is also apparent in their role as oxidases in cardiomyocytes regarding expression level, subcellular localization and their role in physiological and pathological conditions.

In cardiomyocytes, NOX2 is reported to locate to the sarcolemma [102]. It has been shown that NOX2 activity is mainly regulated by angiotensin II (AngII) and endothelin-1 via G-protein coupled receptors (GPCRs), but also by growth factors, cytokines and mechanical stress [103]. These signaling pathways promote phosphorylation of p47phox and subsequently NOX2 complex formation [104].

In contrast, the general subcellular localization of NOX4 has been a subject of debate. For cardiomyocytes, most data suggests that NOX4 is associated with the SR membrane, but it has also been described to be localized in mitochondria as well as intranuclear [105,106].

The last decades have brought increasing evidence that NOX2 and NOX4 are involved in both healthy and pathophysiological processes in cardiomyocytes. NOX2 is described to be involved in the progression of cardiomyocyte hypertrophy and heart failure induced via the renin-angiotensin-aldosterone system, which is a paramount element in the development of heart failure [107]. A physiological role of NOX2 activation has been identified in the context of X-ROS signaling. X-ROS signaling describes the induction of NOX2-dependent ROS production upon

mechanical stretch of cardiomyocytes. In turn, the produced ROS regulates RyR2 channel activation [108]. In the failing heart, NOX4 expression in cardiomyocytes is increased as demonstrated in mouse models of pressure-overloaded hearts. The increase in expression and thus in NOX4 activity has been identified as protective against chronic load-induced stress by promoting angiogenesis in a paracrine signaling pathway [109]. Furthermore, it has been suggested that NOX4 is involved in RyR2 redox-modification and regulation. In skeletal muscle cells, NOX4 produces ROS in direct dependency of the partial pressure of $O_2$, thus acting as a $O_2$ sensor. The generated ROS oxidize RyR1 and increase its activity [110]. Whether this applies for NOX4 and RyR2 in cardiomyocytes remains unclear.

While NOX2 and NOX4 have been recognized as key components in distinct signaling pathways and in overall cardiomyocyte function, the detailed consequences of NOX2- and NOX4-dependent ROS production are only incompletely understood.

## 1.6. Aims of the thesis

Calcium influx via L-type $Ca^{2+}$ channels activates intracellular $Ca^{2+}$ release from the sarcoplasmic reticulum through type 2 ryanodine receptor channels (RyR2) via $Ca^{2+}$ induced $Ca^{2+}$ release (CICR), and facilitates cardiomyocyte contraction. Posttranslational modifications of redox-sensitive cysteine residues of RyR2 channels have been associated with increased channel activity. Dysregulation of this redox signaling pathway may increase the risk of arrhythmia through increased diastolic $Ca^{2+}$ leak. The cardiac isoforms of the NADPH-dependent oxidase, NOX2 and NOX4, have been suggested to oxidize RyR2 channels. While for RyR1, the skeletal muscle isoform, functional cysteine modifications have been identified, the exact mechanisms of RyR2 oxidation and the identity of the cysteine residues remain unknown. We hypothesize that NOX4 is closely associated with RyR2 in the SR membrane, where NOX4-dependent ROS production modulates RyR2 channel activity by specific oxidation. Further, NOX4-dependent regulation of RyR2 may be distinct from RyR2 oxidation by NOX2.

This study was designed to explore direct consequences of RyR2 oxidation by NOX2 or NOX4 via a human embryonic kidney cell model (HEK293A). In this model, cells were transfected to heterologously express RyR2 together with NOX2 or NOX4 and an additional genetically encoded ROS-sensor, HyPer-3. This model will be used to investigate if RyR2 channel activity can be modulated by exogenously added ROS and by NOX-dependent ROS production.

In parallel, isolated primary ventricular cardiomyocytes were transduced with a NOX4-expressing adenoviral construct. This approach will allow an analysis of the subcellular localization of NOX4 by superresolution **ST**imulated **E**mission **D**epletion (STED) nanoscopy and subsequent colocalization analyses. The virally transduced cardiomyocytes will be used to further characterize the postulated interaction of RyR2 and NOX4 by co-immunoprecipitation analysis.

Thirdly, in order to specifically identify cysteine residues in RyR2 that are redox-sensitive to NOX-dependent oxidation, a differential alkylation approach in combination with data independent mass spectrometry was designed and foundational experimental protocols will be established.

# 2. Material and Methods

## 2.1. Material

### 2.1.1. Chemicals

| Name | Company |
|---|---|
| **Acetone** | Sigma |
| **Acetic Acid** | Roth |
| **Acrylamide 2x** | SERVA |
| **Acrylamide/Bis-Acrylamide solution** | Roth |
| **Agarose** | Lonza |
| **Ampicillin** | Roth |
| **Bovine Serum Albumin** | Gibco |
| **Bromophenol blue** | Sigma |
| **calcium chloride** | Sigma |
| **CHAPS** | Roth |
| **Collagenase Type 2** | Worthington |
| **Coomassie Blue G-250** | SERVA |
| **Di-sodiumhydrogen phosphate** | Sigma |
| **Dimethylsulfoxide** | Sigma |
| **Dithiotreitol** | Sigma |
| **Dulbeccos modified eagle medium** | Biochrome |
| **EDTA 0.5 M solution** | AppliChem |
| **EGTA** | Sigma |
| **Ethanol** | Merck Millipore |
| **Fetal Bovine Serium** | Invitrogen |
| **Fetal Calf Serum** | Thermo Fisher |
| **Fluo-4 AM** | Thermo Fisher |
| **Flura-5F** | Thermo Fisher |
| **Glucose** | Sigma |
| **Glycerol** | Roth |
| **Glycin** | Roth |
| **HEPES** | Roth |
| **Hydrochloric acid fuming 37 %** | Roth |
| **Hydrogen peroxide** | Sigma |
| **kanamycin** | Roth |
| **L-Glutathione reduced** | Sigma |
| **LB agar agar** | AppliChem |
| **LB Agar powder** | AppliChem |
| **LB Medium** | AppliChem |
| **Magnesium sulfate monohydrate** | Sigma |
| **Methanol** | Roth |

| | |
|---|---|
| **Milk, powdered blotting grade** | Sigma |
| **Nonidet P40** | USB |
| **Penicillin-Streptomycin** | Sigma |
| **Phosphate bufferd saline** | Gibco, Life technologies |
| **PhosSTOP tablet** | Roche |
| **Pierce Bovine Serum Albumin Standard** | Thermo Fisher |
| **Pluronic Acid, 20 %** | Thermo Fisher |
| **Potassium chloride** | Sigma |
| **Potassium dihydrogenphosphate** | Sigma |
| **Protease Inhibotor tablet** | Roche |
| **rat tail collagen type 1** | Corning |
| **Roti® Block** | Roth |
| **Sodium ascorbate** | Sigma |
| **Sodium chloride** | Sigma |
| **Sodium deoxycholate** | Sigma |
| **Sodium dodecylsulfate** | Roth |
| **Sodium dodecylsulfate (20% solution)** | Roth |
| **Sodium hydroxide solution** | Merck Millipore |
| **ß-mercaptoethanol** | Sigma |
| **Sucrose** | Roth |
| **Tetramethylethylenediamine** | Roth |
| **Tris(hydroxymethyl)aminomethane** | Roth |
| **Triton-X-100** | Sigma |
| **Trypsin** | Sigma |
| **Tween-20** | Sigma |
| **Urea** | Roth |

### 2.1.2. Antibodies

| Target protein | Species | Clonality | Clone | Company | Catalog No. | Dilution WB | Dilution IF |
|---|---|---|---|---|---|---|---|
| **Cav3** | Rabbit | poly | - | Abcam | Ab2912 | 1/1000 | 1/500 |
| **GAPDH** | Mouse | - | - | Biotrend | 5G4Mab6C5 | 1:160000 | - |
| **JPH2** | Rabbit | poly | - | Life technologies | 405300 | 1/1000 | 1/1500 |
| **Myc-tag** | Rabbit | poly | - | Sigma | C3956 | 1/1000 | 1/500 |
| **Myc-tag** | Mouse | mono | 9E10 | Sigma | M4439 | 1/1000 | 1/500 |
| **NOX2** | Mouse | mono | 53 | BD | 1/1000 | 611415 | 1/200 |
| **NOX4** | Rabbit | poly | - | Novus Biological | NB110-58851 | 1/1000 | 1/100 |
| **p22phox** | Rabbit | poly | - | Abcam | Ab75941 | 1/1000 | 1/100 |
| **RyR2** | Mouse | mono | C3-33 | Thermo Scientific | MA3-916 | 1/1000 | 1/500 |
| **RyR2** | Rabbit | poly | - | Sigma | HPA020028 | 1/2500 | 1/500 |

| Protein | Species | Clonality | Company | Catalog no. | Dilution WB | Dilution IF (VCM) |
|---|---|---|---|---|---|---|
| **IRDye 800CW Donkey anti-Mouse IgG** | Donkey | poly | LI-COR | P/N926-32212 | 1:10000 | |
| **IRDye 680RD Donkey anti-Mouse IgG** | Donkey | poly | LI-COR | P/N926-68072 | 1:10000 | |
| **IRDye 800CW Donkey anti-Rabbit** | Donkey | poly | LI-COR | P/N926-32213 | 1:10000 | |
| **IRDye 680RD Donkey anti-Rabbit IgG** | Donkey | poly | LI-COR | P/N926-68073 | 1:10000 | |
| **Goat anti-rabbit STAR 635P** | Goat | poly | Abberior | 2-0012-007-2 | | 1:200 |
| **Goat anti-mouse STAR 635P** | Goat | poly | Abberior | 2-0002-007-5 | | 1:200 |
| **Goat anti-rabbit STAR 580** | Goat | poly | Abberior | 2-0012-005-8 | | 1:200 |
| **Goat anti-mouse STAR 580** | Goat | poly | Abberior | 2-0002-005-1 | | 1:200 |

### 2.1.3. Vectors

| DNA vector | Source |
|---|---|
| **pCMV6-Entry-mNOX2-Myc-DDK** | Origene Technologies |
| **pAAV-AC-mNOX4-Myc-DDK** | Origene Technologies |
| **pcDNA3-hRyR2** | Gift from Prof. Phillip Sasse |
| **pC1-HyPer3** | Gift from Prof. Ivan Bogeski |
| **pBudCE4.1-NOX4-HyPer3** | Cloning |
| **pBudCE4.1-NOX2-HyPer3** | Cloning |

### 2.1.4. Viruses

| Viral vector | Source |
|---|---|
| **pO6A5-CMV-NOX2-IRES-eGFP** | Sirion Biotech |
| **PO6A5-CMV-NOX4-IRES-eGFP** | Sirion Biotech |
| **Ad5-CMV-eGFP** | Sirion Biotech |

### 2.1.5. Cell lines

| Cell lines | |
|---|---|
| **Human embryonic kidney 293A cells** | CRL 1573, ATCC |
| **Adult mouse ventricular cardiomyocytes** | Primary cell isolation |

### 2.1.6. Buffers

| 5x SDS running buffer | |
|---|---|
| **Tris-Base** | 125 mM |
| **Glycine** | 96 mM |
| **SDS** | 17.5 mM |

| 5x Transfer buffer | |
|---|---|
| **Tris-Base** | 125 mM |
| **Glycine** | 96 mM |

| TBS, pH 7.4 | |
|---|---|
| **Tris** | 25 mM |
| **NaCl** | 150 mM NaCl |
| **KCl** | 2.7 mM |

| TBST, pH 7.4 | |
|---|---|
| **Tween 20** | 0.05 % (v/v) in TBS |

| Blocking buffer (Western blot) | |
|---|---|
| **Skimmed milk powder** | 5 % in TBST |

| CHAPS CoIP buffer | |
|---|---|
| **NaCl** | 150 mM |
| **Tris-HCl, pH 7.4** | 50 mM |
| **EDTA** | 1 mM |
| **CHAPS** | 0.15 % (w/v) |
| **$H_2O$** | ad. 50 ml |
| **+ Protease & Phosphatase Inhibitor** | |

| **Alkylation buffer pH 7.0** | |
|---|---|
| **HEPES** | 25 mM |
| **NaCl** | 100 mM |
| **EDTA** | 1 mM |
| **SDS** | 0.1 % (w/v) |
| **NP-40** | 1 % (w/v) |
| **$H_2O$** | ad. 50 ml |
| **+ Protease & Phosphatase Inhibitor** | |

#### 2.1.6.1. Buffers for isolation of adult mouse cardiomyocyte

| **10x Perfusion buffer, pH 7.4** | **Final concentration (in mM)** |
|---|---|
| **NaCl** | 120.4 |
| **KCl** | 14.7 |
| **$KH_2PO_4$** | 0.6 |
| **$Na_2HPO_4$ x 2 $H_2O$** | 0.6 |
| **$MgSO_4$ x 7 $H_2O$** | 1.2 |
| **HEPES** | 10 |
| **$H_2O$** | ad. 1 l |

| **1x Perfusion buffer, pH 7.4** | **Final concentration (in mM)** |
|---|---|
| **10 x Perfusion buffer** | 1x |
| **$NaHCO_3$** | 4.6 |
| **Taurin** | 30 |
| **BDM** | 10 |
| **Glucose** | 5.5 |
| **$H_2O$** | ad. 500 ml |

| **Digestion buffer** | **Final concentration** |
|---|---|
| **Collagenase Type II** | 600 U/ml |
| **CaCl2** | 40 µM |
| **1x Perfusion buffer** | ad. 50 ml |

| **Stopping buffer** | **Final concentration** |
|---|---|
| **BCS** | 10 % (v/v) |
| **CaCl2** | 12.5 µM |
| **1x Perfusion buffer** | ad. 50 ml |

| **Culture medium for isolated myocytes** | **Final concentration** |
|---|---|
| **BSA** | 1 mg/ml |
| **Penicillin** | 100 U/ml |
| **L-Glutamin** | 2 mM |
| **Blebbistatin** | 25 µM |
| **ITS** | 1x |

| | |
|---|---|
| **HEPES** | 10 mM |
| **MEM-Medium** | ad. 50 ml |

### 2.1.7. Kits

| Name | Company |
|---|---|
| **Dynabeads protein G** | Thermo Fisher |
| **Plasmid isolation (mini)** | Qiagen |
| **Plasmid isolation (midi)** | Qiagen |
| **Nucleo Spin Gel and PCR clean-up** | Macherey-Nagel |
| **Pierce™ BCA Protein Assay Kit** | Thermo Scientific |
| **Pierce™ S-Nitrosylation Western Blot Kit** | Thermo Scientific |

### 2.1.8. Instruments

| Name | Company |
|---|---|
| **Absorption/fluorescence plate reader** | Tecan |
| **Blotting Station** | AA Hoeffer |
| **Breeding cabinet (E. coli), Inforst HAT** | Ecotron |
| **Breeding cabinet (cell culture), HERAcell 150i** | Thermo Fisher |
| **Centrifuge** | Sorva |
| **Confocal microscope** | Zeiss |
| **DNA Camera Hero Doc plus** | Herolab |
| **Potter homogenizer RW20 digital** | IKA |
| **Electrophoresis Power Supply** | Bio-Rad |
| **Magnet-stirrer RCT standard** | IKA |
| **Confocal Microscope LSM880** | Zeiss |
| **pH Electrode** | Hannah Instruments |
| **Photometer** | Eppendorf |
| **Pipetboy** | Integra |
| **Pipettes** | Eppendorf/Gilson |
| **Rotating wheel PDR-35** | Grant-bio |
| **Shaker table Duomax 1030** | Heidolph |
| **STED microscope** | Leica |
| **Tabletop centrifuge HERAEUS Pico 17** | Thermo Fisher |
| **Tabletop centrifuge HEAREUS Fresco** | Thermo Fisher |
| **Thermocycler, lab cycler** | SensoQuest |
| **Thermomixer** | Eppendorf |
| **Ultra turrax D1** | Miccra |
| **Ultracentrifuge** | Beckman coulter |
| **Vortexer** | Scientific industries |
| **Waterbath** | Memmert |
| **WB-detection cabinet** | Li-Cor |

### 2.1.9. Consumables

| Name | Company |
|---|---|
| **Eppendorf Tubes 1.5 ml** | Eppendorf |
| **Eppendorf Tubes 2.0 ml** | Eppendorf |
| **Reaction tube 15 ml** | Sarstedt |
| **Reaction tube 50 ml** | Sarstedt |
| **PCR tube 200 µl** | Sarstedt |
| **Pipette tips 10 µl** | Sarstedt |
| **Pipette tips 200 µl** | Sarstedt |
| **Pipette tips 1000 µl** | Sarstedt |
| **Pipette 5 ml** | Sarstedt |
| **Pipette 10 ml** | Sarstedt |
| **Pipette 25 ml** | Sarstedt |
| **Pipette 50 ml** | Sarstedt |
| **Gel Loader Tips** | Sarstedt |
| **Pipette filter tips 10 µl** | Sarstedt |
| **Pipette filter tips 200 µl** | Sarstedt |
| **Pipette filter tips 1000 µl** | Sarstedt |
| **Cell culture flask T25** | Sarstedt |
| **Cell culture flask T75** | Sarstedt |
| **Cell culture flask T175** | Sarstedt |
| **6-well plate** | Greiner |
| **12-well plate** | Greiner |
| **24-well plate** | Greiner |
| **96-well plate** | Greiner |
| **Immobilon-P PVDF Membrane 0.45 µm** | Merck Millipore |
| **Immobilon-FL PVDF Membrane 0.45 µm** | Merck Millipore |
| **Sterile filter** | Millipore |
| **Sterile filter for buffer** | Millipore |
| **Cannula, 27G** | Braun |
| **Cannula, 20G** | Braun |
| **Cell scraper** | Sarstedt |
| **Low profile 96 well plate** | Bio-Rad |
| **syringe 1 ml** | Braun |
| **ultracentrifuge tube I** | Beckman |
| **ultracentrifuge tube II** | Beckman |

### 2.1.10. Software

| Name | Company |
|---|---|
| **Word** | Microsoft Inc. |
| **PowerPoint** | Microsoft Inc. |

| | |
|---|---|
| **Excel** | Microsoft Inc. |
| **Fiji Image** | https://imagej.net/Fiji |
| **Prism (Version 7.03)** | GraphPad |
| **VisiView imaging software** | Visitron Systems GmbH |
| **LAS X imaging software** | Leica Microsystems |
| **Image studio 5.0** | LI-COR |

## 2.2. Methods

### 2.2.1. Cell biological methods

#### 2.2.1.1. Mouse husbandry

Mice (C57Bl/6N) were housed at the central animal facility (ZTE) of the University Medical Center Göttingen. Animal cages were equipped with nesting material, with food and water provided ad libitum. Cages were ventilated individually (IVC) and animal rooms were kept at 20-24°C and 45-65% rel. humidity, with constant day/night cycles of 12 h each. All animal procedures were reviewed by the Institutional Animal Care and Use Committee by the University Medical Center Göttingen and approved by veterinarian state authority (LAVES, Oldenburg, Germany) in compliance with the humane care and use of laboratory animal policy (33.9-42502-04-16/2102). If not stated otherwise, male or female wt mice, age12-16 weeks, were used.

#### 2.2.1.2. Mouse cardiomyocyte isolation

Isolation of adult murine ventricular cardiomyocytes was performed according to a protocol by Wagner et al. [111]. In short, mice were anaesthetized by isoflurane inhalation and sacrificed by cervical dislocation. After removal of the heart, a 21-gauge cannula was inserted into the aorta and the cannulated heart was connected to a modified Langendorff perfusion setup [112]. Perfusion buffer (see 2.1.6.1) was used to wash out remaining blood by retrograde perfusion. After 4 minutes of washing, perfusion buffer was replaced with digestion buffer and digestion was carried out for 9 min at 37°C. By cutting the heart just below the atria, the ventricles were removed and placed in a small dish containing digestion buffer. The tissue was cut into small pieces using scissors. By carefully pipetting up and down, ventricular cardiomyocytes were isolated. Stop buffer was added to inactivate the digestion and the cell suspension was transferred to a 15 ml tube. After washing the cells three times with stop buffer, they were either subjected to immunocytochemistry (2.2.1.7), short-term cell culture (2.2.1.3) or immediately frozen for biochemical applications.

#### 2.2.1.3. Short-term primary cell culture

For viral transduction of isolated ventricular cardiomyocytes, cells were put into cultivation for 48 h. Directly after isolation (2.2.1.2), ventricular cardiomyocytes were incubated in stop buffer with increasing $Ca^{2+}$ concentrations for 8 min each (100 µM, 400 µM and 900 µM, respectively). In a last step, cells were resuspended in cell culture medium (2.1.6.1), plated 6-well dishes, and incubated at 37°C with 5 % $CO_2$.

#### 2.2.1.4. Viral transduction of cardiomyocytes

For induction of overexpression of proteins of interest in isolated cardiomyocytes, cells were isolated and put into short-term cell culture as described above (see 2.2.1.2 and 2.2.1.3). 24 hours after isolation, cell culture medium was exchanged with medium containing virus. For that virus stock solution was diluted in cell culture medium until the sufficient multiplicity of infection (MOI) was achieved. Viral load was tested using a variety of MOIs and an MOI of 1000 was chosen as it resulted in stable expression of the eGFP transfection control in more than 70 % of the cells. Cells were incubated for 48 hours, after which cells were subjected to further analysis.

#### 2.2.1.5. HEK293A cell culture

Cells were cultivated at 37°C and 5% $CO_2$ with saturated humidity. Cells were split every 3-4 days in a ratio of 1:10. For that, the medium was removed, and cells were washed with PBS once. Cells were treated with 1x trypsin for 1-2 minutes at 37°C. By adding a five-fold amount of fresh medium, trypsin activity was stopped. This also detached the cells from the culture vessel. The cell suspension was transferred into a 15 ml centrifuge tube and centrifuged for 5 minutes at 500x g. The cell pellet was resuspended in culture medium and the appropriate cell amount was seeded into a new, fresh medium containing culture vessel.

#### 2.2.1.6. Cell transfection

Cell were chemically transfected to specifically overexpress proteins for further functional or biochemical assays. In short, cells were grown to a confluency of 70-80 %. For transfection using Lipofectamine 3000 (Lipofectamine 3000 Transfection Reagent, Invitrogen), two mixes were prepared separately as follows:

**Mix A)**

| | |
|---|---|
| **Lipofectamine** | 3 µl per µg DNA |
| **DMEM** | ad. 500 µl |

**Mix B)**

| | |
|---|---|
| **P 3000** | 5 µl per µg DNA |
| **Nucleic acid (plasmid DNA)** | - |
| **DMEM** | ad. 500 µl |

The individual mixes were vortexed vigorously and incubated for 5 min. Next, the mixes were combined and incubated further for 30 min. The combined mix was then added to the cells and incubated for at least 24 hours. The next day, the transfection medium was exchanged for normal growth medium, and cells were subjected to further assays.

#### 2.2.1.7. Immunocytochemistry

Immunocytochemistry was used to stain proteins of interest in isolated cardiomyocytes, transfected HEK293A cells or virally transduced isolated cardiomyocytes. In general, cells were seeded on rat-tail collagen (HEK293A cells) or laminin-coated (isolated cardiomyocytes) glass coverslips. After fixation of cells by incubation in 4 % PFA for 10 min, cells were incubated permeabilization/blocking buffer (0.2 % Triton-X 100, 10 % BCS in PBS) overnight. Next, cells were incubated with the primary antibody diluted in permeabilization/blocking buffer as indicated in the antibody table (2.1.2, see "dilution IF"). To remove the antibody, cells were washed three times with permeabilization/blocking buffer. After that, cells were incubated with secondary antibodies diluted in permeabilization/blocking buffer overnight. Again, cells were washed three times with permeabilization/blocking buffer and coverslips were mounted on glass object slides and subjected to STED nanoscopy.

#### 2.2.1.8. STED nanoscopy

**ST**imulated **E**mission **D**epletion (STED) microscopy was performed following previously published protocols [113]. For STED nanoscopy, a Leica TCS SP8 STED system with a HC PL APO C2S 100x/1.40 oil immersion objective was used [114]. STED images were acquired using a pixel size of 16.23 x 16.23 nm, a pixel dwell time of 400 ns, a scanning speed of 600 Hz, 32x line averaging, fluorophore excitation by a white-light laser at 635 and 580 nm, STED depletion at 775 nm, and fluorescence detection between 650-700 nm and 600-630 nm [114]. The STED laser beam was adjusted to optimize the STAR 635P and STAR 580 signal resolutions. Raw images were processed 6 in ImageJ [114].

#### 2.2.1.9. Functional calcium imaging

Functional calcium imaging was performed to monitor $Ca^{2+}$ handling in RyR2-transfected HEK293A cells at an epifluorescence microscopy setup using $Ca^{2+}$-sensitive fluorescent dyes. For HEK293A cell transfection 100.000 cells were seeded onto glass-bottom microscopy dishes 24 h prior to transfection. The transfection was performed as described above (2.2.1.6), with 2 µg plasmid DNA being used. For visualization of changes in intracellular $Ca^{2+}$ concentrations, Fluo4-AM and Fura-5F (Invitrogen, Thermo Fisher) were prepared as a 1 mM stock using 20 % Pluronic acid (Thermo Fisher). HEK293A cells were incubated with either 10 µM Fluo4-AM or Fura-5F in $Ca^{2+}$-Tyrode solution for 30 min. After washing the cells three times with $Ca^{2+}$-Tyrode solution, cells were subjected to epifluorescence microscopy. Changes of extracellular $Ca^{2+}$ concentrations were introduced 15 min prior to microscopy. In cases where $Ca^{2+}$ concentrations were changed during microscopy, a superfusion system was used and $Ca^{2+}$ concentrations were changed in 5-, or 10-min intervals.

| $Ca^{2+}$-Tyrode solution (pH 7.4) | Concentration (in mM) |
|---|---|
| **NaCl** | 140 |
| **HEPES** | 10 |
| **Glucose** | 10 |
| **$Na_2HPO_4$** | 0.33 |
| **$MgCl_2$** | 1.2 |
| **KCl** | 5.4 |
| **$CaCl_2$** | 1.8 |

## 2.2.2. Biochemical methods

### 2.2.2.1. Protein concentration determination assay

To determine the protein concentration in a sample, a bicinchoninic acid (BCA) assay was performed according to the protocol provided by manufacturer (Pierce, Thermo Fisher). For that, a protein standard with known protein concentrations was prepared as follows:

| Vial | Volume diluent | Volume BSA stock (2 mg/ml) | Final BSA concentration (µg/µl) |
|---|---|---|---|
| **A** | 0 | 300 | 2000 |
| **B** | 125 | 375 | 1500 |
| **C** | 325 | 325 | 1000 |
| **D** | 175 | 175 | 750 |
| **E** | 325 | 325 | 500 |
| **F** | 325 | 325 | 250 |
| **G** | 325 | 325 | 125 |
| **H** | 400 | 100 | 25 |
| **I** | 400 | 0 | 0 |

***Table 1: Protein standards for BCA assay.***

25 µl of each standard and an appropriate dilution of the tested sample (in duplicates) were pipetted into a 96-well plate. Component A and component B were mixed (200 µl/per sample of A; 4 µl/per sample of B), and 200 µl of this mix was added to the samples. After an incubation for 30 min at 37°C the extinction at 562 nm was measured using the TECAN plate reader. The protein standards were then used for calibration and sample protein concentration was calculated accordingly.

### 2.2.2.2. SDS-PAGE

The SDS-PAGE (sodium dodecyl sulfate-polyacrylamide gel electrophoresis) is a method to separate proteins according to their molecular weight. SDS causes denaturation (secondary and non-disulfide-linked tertiary structures) of proteins and applies a negative charge to each protein. The polyacrylamide gel serves as the separating matrix. Polyacrylamide gels were either

prepared freshly or commercially available precast gels were used (Novex, Tris-Glycine gels, 4 – 20 % gradient, Thermo Fisher). For preparation of separating acrylamide gels, components were mixed as follows:

| **Gel percentage** | **6 %** | **7.5 %** | **8 %** | **10 %** | **12 %** | **13.5 %** | **15 %** |
|---|---|---|---|---|---|---|---|
| Acrylamide/Bisacrylamide (ml) | 2.4 | 3 | 3.2 | 4 | 4.8 | 5.4 | 6 |
| 4x Tris/SDS, pH 8.8 (ml) | 3 | 3 | 3 | 3 | 3 | 3 | 3 |
| $H_2O$ | 6.6 | 6.3 | 5.8 | 5 | 4.2 | 3.6 | 3 |
| APS, 10% (µl) | 48 | 48 | 48 | 48 | 48 | 48 | 48 |
| TEMED (µl) | 18 | 18 | 18 | 18 | 18 | 18 | 18 |

***Table 2: Composition of separating acrylamide gels with varying percentages.***

To load samples onto the gel, a collecting acrylamide gel was added on top of the separating gel with components mixed as follows:

| | |
|---|---|
| Acrylamide/Bisacrylamide (ml) | 1 |
| 4x Tris/SDS, pH 6.8 (ml) | 1.88 |
| $H_2O$ (ml) | 4.62 |
| APS, 10 % (µl) | 37.5 |
| TEMED (µl) | 15 |

***Table 3: Composition of collecting acrylamide gel.***

After loading of samples and a molecular weight marker (PageRuler Prestained protein ruler, Thermo Fisher), the acrylamide gels were mounted into the electrophoresis chamber. Both inner and outer chamber were filled with 1x SDS running buffer (see 2.1.6). The electrophoresis was performed at 200 V for 50 min. After completion, the gel was subjected to Western blot analysis (see 2.2.2.3).

#### 2.2.2.3. Western blot analysis

Western blot is a method used to immobilize proteins on a membrane to perform subsequent steps of analysis. Therefore, a polyacrylamide gel from an SDS-PAGE (see 2.2.2.2) was placed on a polyvinylidene fluoride (PVDF) membrane. The proteins separated during SDS-PAGE were transferred to the membrane via electrophoresis in a tank system using 1x transfer buffer (see 2.1.6). The transfer was carried out at 4°C at 100 V for one hour. Once finished, the membrane was washed in TBS and TBST each for ten minutes before it was incubated with blocking buffer (see 2.1.6) for 1 hour at room temperature. Thereafter, the membrane was incubated with the primary antibody in an appropriate dilution in blocking buffer overnight at 4°C on a shaker. The membrane was then washed 5 times for 5 minutes in TBST. After this, the membrane was incubated with the appropriate secondary antibody (IRDye 800CW, IRDye 680RD, LI-COR Biosciences) diluted in blocking buffer for 1 hour at room temperature before it was washed 5

times for 5 minutes with TBST. The proteins were detected using the Odyssey CLx imaging system (LI-COR Biosciences).

#### 2.2.2.4. Co-immunoprecipitation

To investigate potential direct or indirect protein-protein interactions, co-immunoprecipitation assays followed by Western blot analysis were performed. In general, cells or tissue were lysed in CoIP buffer (10 µl buffer/mg cells or tissue) (2.1.6). Lysates were homogenized using a glass potter (40 strokes at 2000 rpm, on ice). After that, the suspension was aspirated 10x through a G37 needle. Following centrifugation for 10 min at 5000x g at 4°C, the supernatant was transferred to a new tube and the protein concentration was determined (2.2.2.1). 500 µg of total protein was used for CoIP. Samples were mixed with 4 µg of a specific primary antibody or an unspecific normal IgG antibody serving as a negative control (see 2.1.2). After overnight incubation at 4°C, the lysate-antibody mix was added to 30 µl pre-washed DynaBeads and incubated at 4°C for 90 min. Following three washing steps with CoIP buffer for 10 min each, proteins were eluted by addition of 2x sample buffer and incubation for 10 min. DynaBeads were removed using a magnetic rack. Samples were subjected to Western blot analysis (2.2.2.3).

#### 2.2.2.5. Differential alkylation

For the identification of oxidized cysteine residues, a differential alkylation protocol was established. HEK293A wt cells were harvested and lysed in alkylation buffer (2.1.6). After pottering and lysate clearing by centrifugation for 5 min at 5000x g, a small volume of cell lysate was separated and used for protein concentration determination (2.2.2.1). Protein concentrations were adjusted to yield 1 - 2 µg/µl of total protein. For the first alkylation, IAM was added to the lysate (final IAM concentration: 66 mM) and samples were incubated for 30 min in darkness. For removal of IAM, samples were loaded into 5-kDa cut-off centrifugation columns and centrifuged three times for 12 min each at 12.000x g. Between each centrifugation step the volume of the samples was replenished with alkylation buffer. After removal of IAM, samples were reduced by addition of 10 mM TCEP. Excess of TCEP was removed by using the 5-kDa cut-off centrifugation columns as described above. For the second alkylation, NEM was added (final concentration: 10 mM) and samples were incubated for 30 min in darkness. Afterwards, NEM was removed by using the again. To stop the alkylation reaction an excess of β-mercaptoethanol was added to the samples (final concentration: 20 mM). Finally, 5x SB buffer was added and samples were subjected to data-independent mass spectrometry.

For label-free SWATH-MS quantification samples were run on 4-12 % gradient gels, cut out as a single fraction, and in-gel trypsin digested. Rabbit IgG (12-370, Merck) was used as negative control. Digested proteins were planned to be analyzed with a nanoflow chromatography system

(Eksigent nanoLC425, SCIEX) hyphenated to a hybrid triple quadrupole-TOF mass spectrometer (TripleTOF 5600+, SCIEX) equipped with a Nanospray III ion source.

#### 2.2.2.6. Statistical analysis

Data were represented as mean ± standard error of the mean (SEM). The unpaired two-tailed students t-test and ANOVA analyses were used, considering a p-value of less than 0.05 as statistically significant. Details are noted at the individual experiments. Prism (Vers. 7.03, GraphPad) was used for all statistical analyses.

# 3. Results

## 3.1. Evaluation of NOX4 antibodies

For conclusive results of many biochemical assays, such as Western blot analysis or immunocytochemistry, antibody validation is key. For that reason, a rabbit polyclonal antibody from Novus Biological (NB) and a rabbit monoclonal antibody from Abcam raised against NOX4 were tested and compared against a NOX4 antibody already established in the literature (see *Anilkumar et al., ATVB, 2008*), which was raised against 12 C-terminal peptides (556-568) of NOX4 (Figure 5) [115]. Similarly, the epitope for the antibody from NB is located in the C-terminus of NOX4 as well. Generally, the epitope of all tested antibodies is present in all NOX4 splice variants.

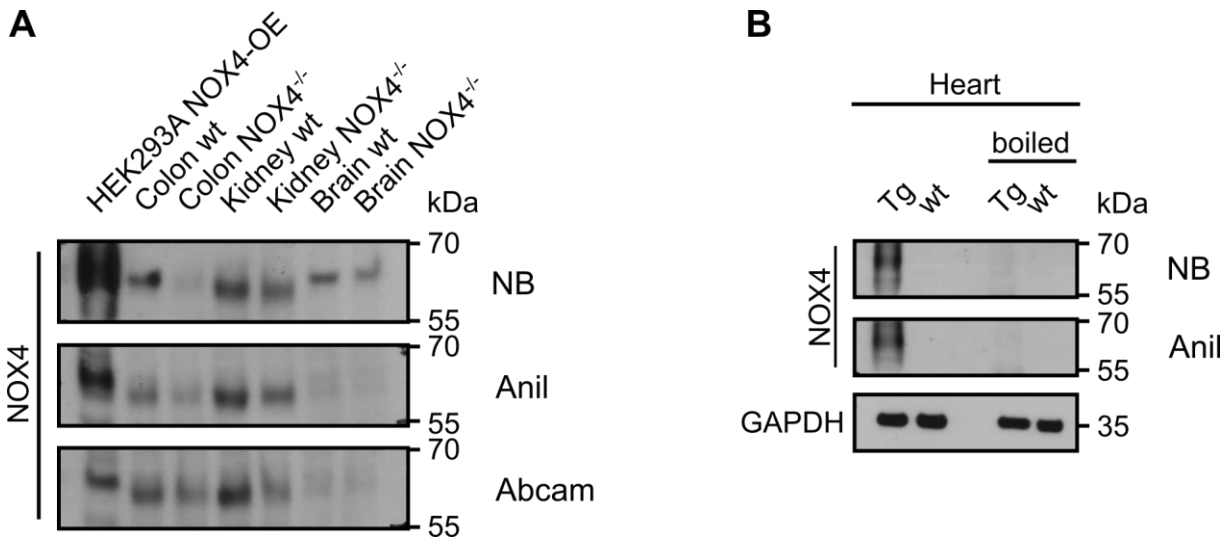


***Figure 5: NOX4 antibody validation in different tissues.***

***A)*** *Colon, kidney, and brain tissue from wt and NOX4$^{-/-}$ was harvested and subjected to SDS-PAGE and consecutive Western blot analysis. HEK293A cells overexpressing NOX4 were used as a positive control. For detection of NOX4, two commercially available (Novus Biological (NB) and Abcam (ab109225) and one non-commercial antibody (Anil, see Anilkumar et al., ATVB, 2008) were tested, which was raised against 12 C-terminal peptides (556-568). All three antibodies were suitable to detect a NOX4 specific signal at around 60 kDa, with the NB antibody featuring the strongest signal. NOX4$^{-/-}$ samples (lacking exon 14 and 15 of NOX4, Kleinschnitz et al., PLOS, 2010) are not suitable for antibody evaluation, since NOX4 was still detectable with all tested antibodies.* ***B)*** *Heart tissue from wt and NOX4-transgenic (Tg) mice were used to test if the antibodies can detect NOX4 in heart samples. Both tested antibodies could detect elevated NOX4 levels in NOX4-transgenic heart tissue, but not base-line levels in wt tissue. Boiling of the samples abrogated the detection of NOX4 signal. GAPDH was used as a loading control.*

Tissues with high expression of NOX4 from wt and NOX4$^{-/-}$ mice were used as positive controls for the evaluation of the antibodies. For that, tissues were lysed and subjected to SDS-PAGE and Western blot analysis (see 2.2.2.2 and 2.2.2.3). NOX4$^{-/-}$ mice lacking exon 14 and 15 of the enzyme are constitutively NOX4-deficient [116]. Additionally, HEK293A cells overexpressing NOX4 were used as a positive control (Figure 5A). Both commercially available antibodies (NB and Abcam) as well as the non-commercial NOX4-specific antibody were able to detect a signal at 65 kDa, which is the reported size for NOX4 [117]. As all antibodies detected a signal in NOX4$^{-/-}$ tissue, the specific binding epitope of the antibodies is still present in NOX4$^{-/-}$ lacking only exons 14 and 15. Since the NB antibody showed the strongest signal and detected NOX in brain lysates, it was used for all further experiments unless indicated otherwise. Next, heart tissue from wt and NOX4-transgenic (i.e. NOX4-overexpressing [109]) mice were used to examine cardiac NOX4 expression. Both tested antibodies could detect elevated NOX4 levels in NOX4-transgenic left and right ventricular heart tissue, but notably not the baseline levels in wt tissue (left and right ventricles). Boiling of the samples abrogates the detection of NOX4 signal as expected (Figure 5B).

## 3.2. Functional analysis of NOX/hRyR2 interaction in HEK293A cells

### 3.2.1. Establishment of the HEK293A cell model

To directly investigate a potential regulatory impact of NOX-dependent ROS production on RyR2 channel function, a HEK293A cell model was established. For a transient overexpression of the human isoform of RyR2 (hRyR2) and NOX2 or NOX4, cells were transfected according to the protocol described above (see 2.2.1.6). Cells were harvested 48 h after transfection and subjected to SDS-PAGE and Western blot analysis (Figure 6). Individual transfection of HEK293A cells with 1 µg plasmid DNA for NOX2, NOX4 or hRyR2 resulted in expression of these proteins (Figure 6A/B). The used antibodies for NOX2 and NOX4 showed no cross-reactivity. Both proteins could also be detected via their C-terminal Myc-tag. Transfection with both NOX2 and NOX4 concomitantly increased endogenous expression levels of p22phox (Figure 6A), the

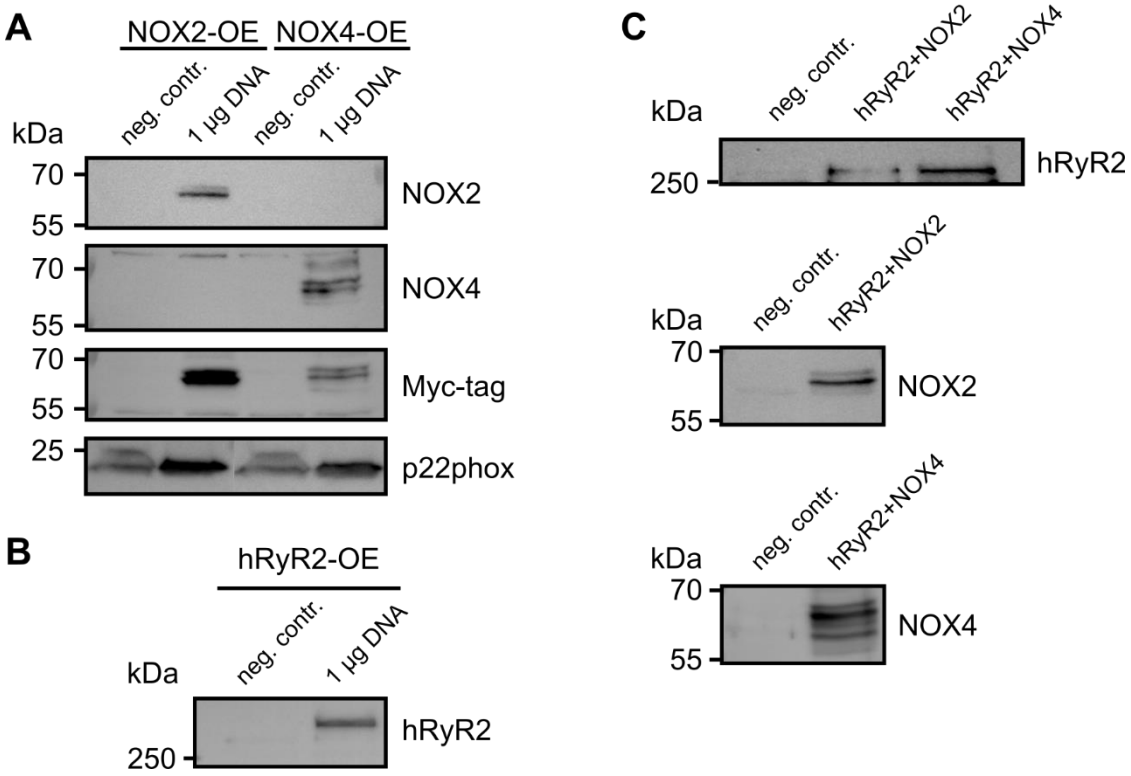


***Figure 6: Overexpression of NOX2, NOX4 and hRyR2 in HEK293A cells.***

*HEK293A cells were transfected with 1 µg of either NOX2, NOX4* ***(A)*** *or hRyR2* ***(B)****. Protein levels were analyzed by Western blot. NOX2 and NOX4 were detected by both NOX2- and NOX4-specific antibodies as well as a myc-antibody against the C-terminal myc-tag of NOX2 and NOX4. Transfection with either NOX2 or NOX4 also elevated expression levels of endogenous p22phox in HEK293A cells.* ***C)*** *Double-transfection of HEK293A cells with both NOX2 and hRyR2 or NOX4 and hRyR2 resulted in the expression of both proteins. Representative blots (n=>5) are shown. 40 µg of total protein was loaded.*

essential subunit for enzymatic function. Double-transfection of HEK293A cells with either NOX2 and hRyR2 or NOX4 and hRyR2 resulted in expression of both proteins.

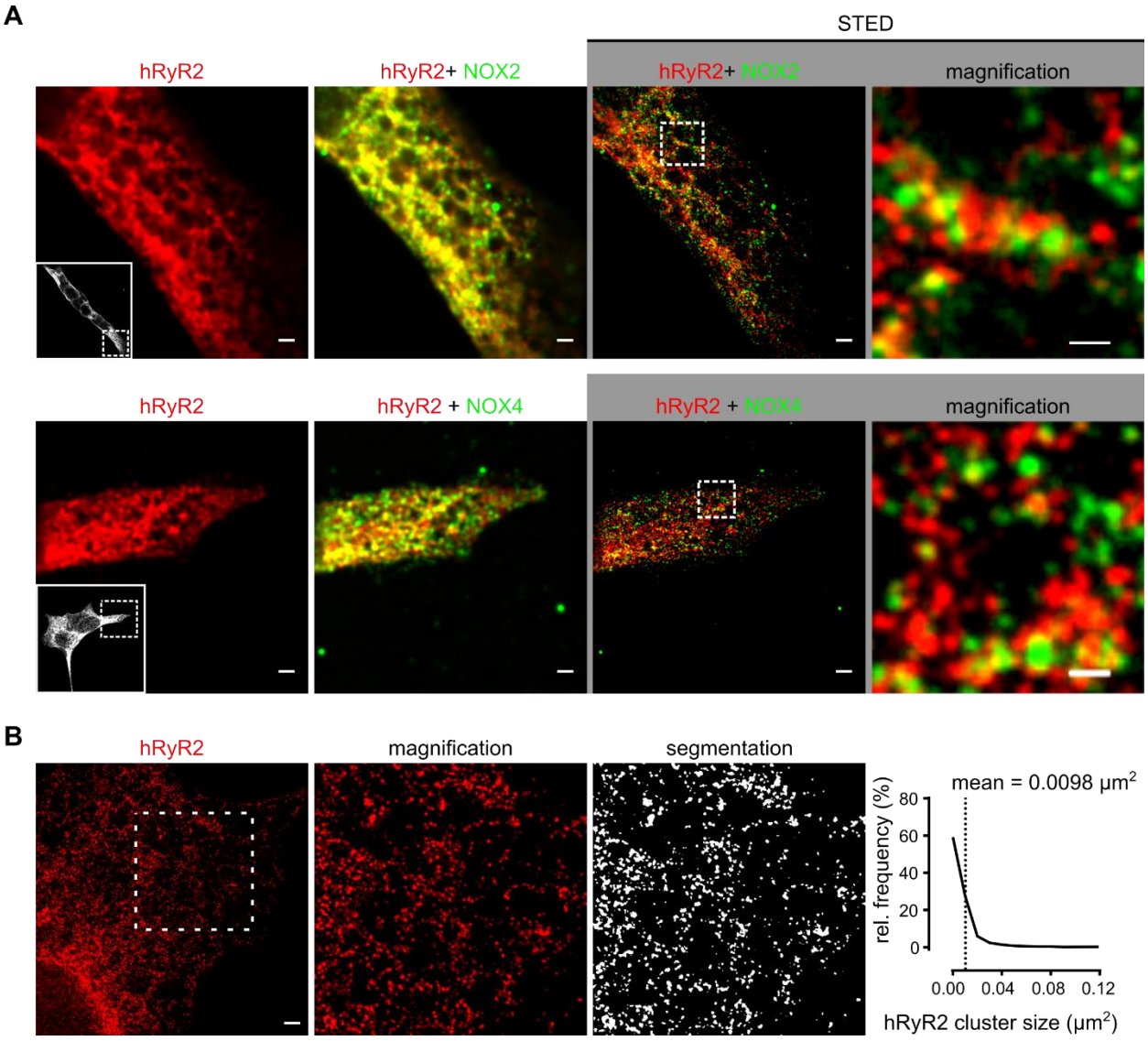


***Figure 7: Confocal and STED microscopy reveal close association of NOX2 and NOX4 with hRyR2 in HEK293A cells.***

***A)*** *Co-transfected HEK293A cells were stained for NOX2 or NOX4 and hRyR2 and subjected to fluorescence microscopy. Dashed boxes indicate areas further analyzed by superresolution STED nanoscopy. Fluorescence signals for hRyR2 (red) and NOX2 or NOX4 (green) show a close association of NOX proteins with hRyR2.* ***B)*** *hRyR2 cluster size was analyzed in hRyR2-transfected HEK293A. STED immunofluorescence images stained for hRyR2 were segmented using Fiji. hRyR2 images were background subtracted (rolling ball radius: 30 pixels), smoothed (Gaussian, sigma 1 pixel), and global Otsu thresholding was used to binarize the hRyR2 signals. Using the binarized images, particle sizes were calculated and displayed according to their relative frequency (n=8). Scale bar = 1 µm; magnification: scale bar = 0.2 µm)*

As subcellular localization of the overexpressed proteins is important for the potential regulatory impact of NOX on RyR2, immunocytochemistry of transfected HEK293A cells was performed (Figure 7). In short, HEK293A cells were transfected with either NOX2 and hRyR2 or NOX4 and hRyR2. 48 h after transfection, cells were fixed using 4% PFA and incubated with primary antibodies against NOX2, NOX4 and hRyR2, respectively. Cells were then incubated with secondary antibodies and subjected to fluorescence microscopy. Confocal imaging (Figure 7A, two left panels) exhibited distinct overlap of fluorescence signals for hRyR2 (red) and NOX2 or NOX4 (green), respectively. Signals for hRyR2, NOX2 or NOX4 appeared to be distributed in a reticular fashion, indicating an ER-localization in HEK293A cells. Using the higher spatial resolution of STED nanoscopy (Figure 7A, two right panels), imaging revealed individual signal clusters for both hRyR2 and NOX2 or NOX4, respectively. These clusters appeared to be associated in close proximity but did not overlap.

As cluster size of RyR2 is directly connected to the regulation of $Ca^{2+}$ channel activity of single RyR2 channels within these clusters, STED images of hRyR2-transfected HEK293A cells were used to analyze hRyR2 cluster size in this HEK293A cell model (Figure 7B) [16]. For that, images of hRyR2 fluorescence stains were processed using the Fiji image processing software. In short, images were background subtracted and a Gaussian blur filter was applied. Finally, images were segmented using the Otsu global thresholding algorithm. Cluster size (in $\mu m^2$) of hRyR2 was then

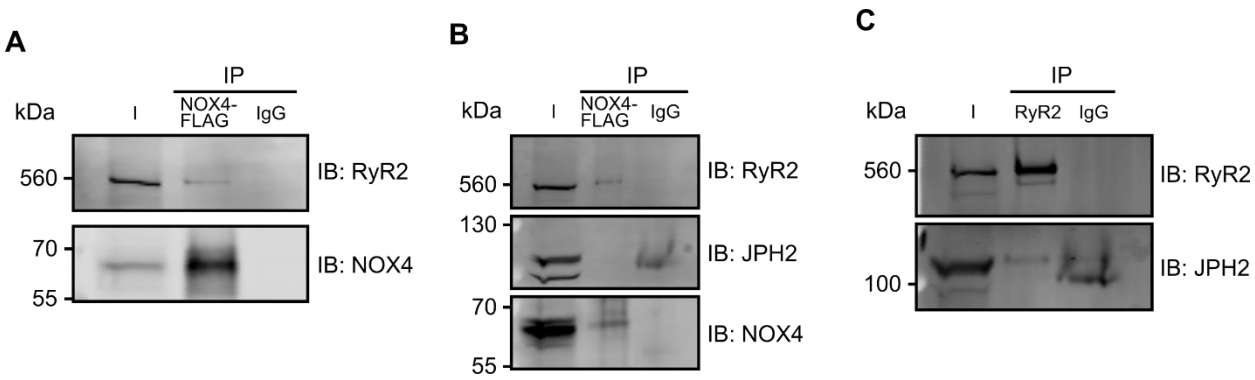


***Figure 8: NOX4 co-immunoprecipitation with RyR2 but not with JPH2 in co-transfected HEK293A cells.***

*HEK293A cells were co-transfected with NOX4, Junctophilin2 (JPH2) and RyR2 (1 µg plasmid DNA each). After 24h of transfection, cells were harvested, and co-immunoprecipitation experiments were performed. Cell lysate was incubated with a* ***A,B)*** *monoclonal FLAG antibody or* ***C)*** *RyR2 antibody to immunoprecipitate NOX4 (C-terminal FLAG-tag) or RyR2, respectively.* ***A)*** *Immunoprecipitation of NOX4 results in a co-precipitation of RyR2.* ***B)*** *RyR2, but not JPH2 as a specificity control was co-immunoprecipitated with NOX4.* ***C)*** *JPH2 was co-immunoprecipitated with RyR2 (IP= immunoprecipitation, I= Input, IB= Immunoblot).*

calculated resulting in a mean cluster size of 0.0098 $\mu m^2$. The relative distribution of hRyR2 cluster sizes also showed an abundance of small clusters.

Immunofluorescence imaging demonstrated that hRyR2 is closely associated with NOX2 and NOX4. As NOX4 as well as RyR2 are described to be localized in the endo/sarcoplasmic reticulum of cells, a co-immunoprecipitation assay was performed to investigate if the close association of NOX4 and hRyR2 in the HEK293A cell model is facilitated by a direct or indirect protein-protein interaction (Figure 8). To do so, HEK293A cells were transfected with NOX4, Junctophilin2 and hRyR2. After harvesting, cell lysates were incubated with a FLAG-antibody targeted against the C-terminal FLAG-tag of NOX4 or an unspecific IgG antibody serving as a negative control. Immunoprecipitated proteins were then pulled down using magnetic beads. Finally, proteins were eluted from the beads and subjected to SDS-PAGE and Western blot analysis (2.2.2.4). Here, RyR2 was co-purified with NOX4 (Figure 8A). Reliability of co-immunoprecipitation protocols depends on selection of appropriate lysis and washing conditions to prevent false negative or false positive results. For this reason, Junctophilin2 (JPH2) was included in this study serving as a specificity control. JPH2 is a reported interaction partner of RyR2 but not NOX4 [118]. Accordingly, RyR2 but not JPH2 was co-purified with NOX4 in triple-transfected HEK293 cells (Figure 8B). Simultaneously, the interaction of RyR2 and JPH2

could be preserved with this protocol. Using a RyR2-specific antibody, JPH2 could be co-purified (Figure 8C).

### 3.2.2. Functional ROS and $Ca^{2+}$ measurement in the HEK293A cell model

To further examine the potential regulatory impact of NOX-dependent ROS production on RyR2 channel function, functional $Ca^{2+}$ measurements in HEK293A cells were performed. For that, hRyR2-expressing HEK293A cells were subjected to epifluorescence microscopy (see 2.2.1.9). In brief, transfected HEK293A cells were loaded with the $Ca^{2+}$-sensitive fluorescent dye Fluo4, with which changes in intracellular $Ca^{2+}$ concentrations were monitored at a live-cell epifluorescence microscopy setup (Figure 9). While non-transfected control cells showed no change in intracellular $Ca^{2+}$ levels (Figure 9A), hRyR2-expressing HEK293A cells exhibited spontaneous periodic $Ca^{2+}$ release waves over the time course of the experiment (Figure 9B). These $Ca^{2+}$ release events could be interrupted by addition of 10 µM ryanodine, a RyR2-specific inhibitor (Figure 9C). To test if these $Ca^{2+}$ release events can be modulated by (NOX-dependent) oxidation of hRyR2, transfected and Fluo4-loaded cells were monitored before and after addition of 1 mM $H_2O_2$ for 5 min each (Figure 10). The frequency of $Ca^{2+}$ release events increased significantly after addition of hydrogen peroxide (Figure 10A). This was also evident in a significant decrease of the mean period time between two consecutive $Ca^{2+}$ release waves, calculated by averaging the time between the fluorescence maxima of these $Ca^{2+}$ release events (Figure 10B).

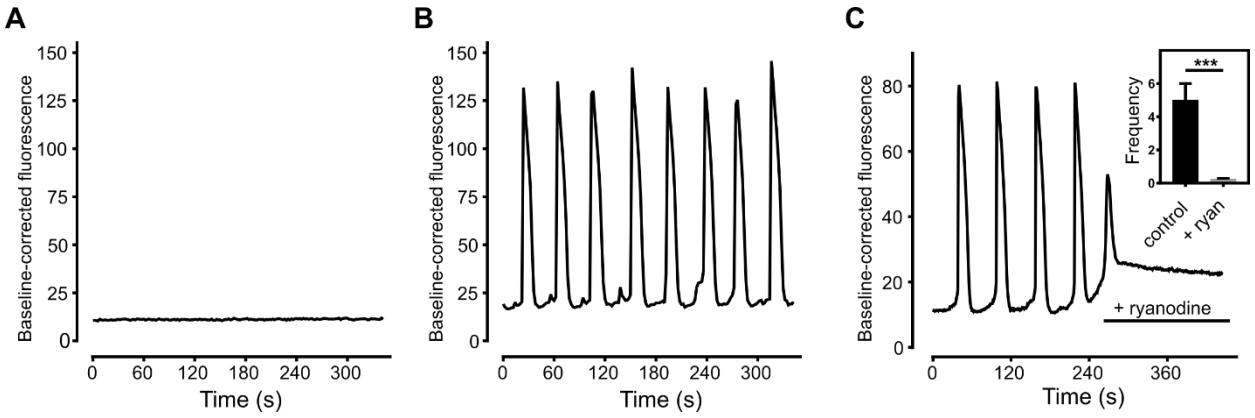


***Figure 9: hRyR2-transfected HEK293A cells exhibit spontaneous $Ca^{2+}$ release events.***

*Live-cell epifluorescence microscopy of HEK293A cells expressing hRyR2* ***(B)*** *show $Ca^{2+}$ release events, that are not present in non-transfected control cells* ***(A)****. Addition of the RyR2-specific inhibitor ryanodine (10 µM) interrupts $Ca^{2+}$ release* ***(C)****. Non-transfected or hRyR2 (1 µg) transfected cells were loaded with 10 µM Fluo4 for 30 min. Cells were recorded at 40x magnification by epifluorescence microscopy. Images were taken once per second (excitation Fluo4: 490 nm, emission 510 nm, exposure: 25 ms, ***p<0.001 with n=3)*

To investigate if NOX2 and NOX4 exert their function as ROS-producing enzymes in this model system, HEK293A cells were additionally transfected with a genetically encoded fluorescence sensor for $H_2O_2$, HyPer-3. These double-transfected cells were monitored using epifluorescence microcopy (Figure 11B). As HyPer-3 is a ratiometric sensor, fluorescence of HyPer-3/NOX-transfected HEK293A cells was monitored at 420 nm and 500 nm. The resulting HyPer-3 ratio (500/420 nm) was significantly increased in HEK293A cells co-transfected with either NOX2 or NOX4 compared to only HyPer-3-transfected control cells (Figure 11B). This indicates a more oxidized intracellular environment. Summarizing, the results presented here describe the establishment of a useful cell model for the investigation of RyR2 channel activity.

Since transfection rates were a limiting factor in the generation of hRyR2/NOX-transfected HEK293A cells additionally expressing HyPer-3, a cloning strategy was developed to combine NOX2 or NOX4 with HyPer-3 on a single plasmid. Using the pBudCE4.1 vector backbone for the final construct, individual expression of the NOX enzymes and HyPer-3 is ensured (for vector maps see Figure 20).

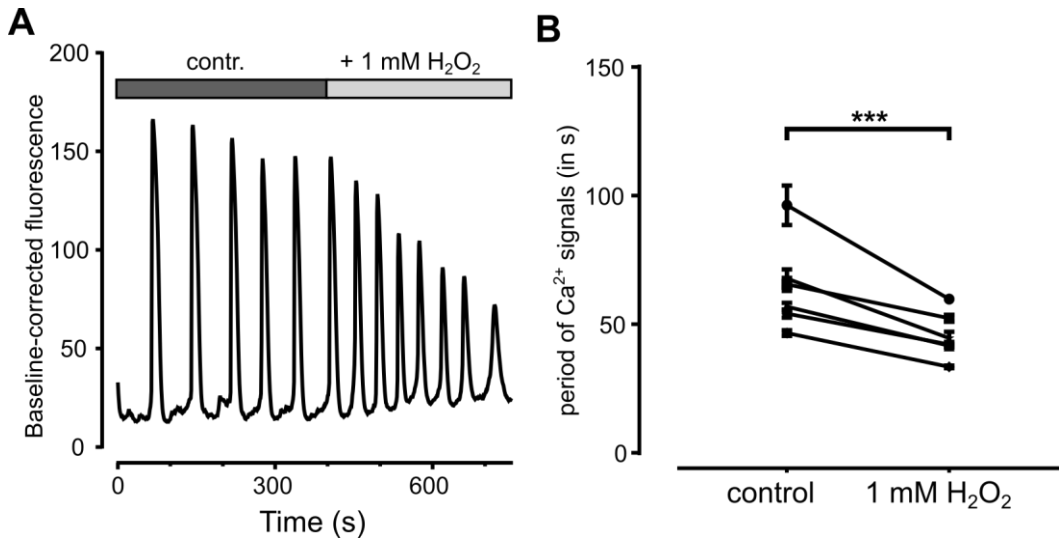


***Figure 10: Hydrogen peroxide increases $Ca^{2+}$ release event frequency of hRyR2-expressing HEK293A cells.***

***A)*** *hRyR2 (1 µg) transfected cells were loaded with 10 µM Fluo4-AM for 30 min. Cells were recorded at 40x magnification by epi-fluorescence microscopy. Initially, cells were incubated with Tyrode's solution containing 1.8 mM $Ca^{2+}$. After 5 min solution was changed for Tyrode's solution supplemented with 1 mM $H_2O_2$.* ***B)*** *Mean period time between consecutive $Ca^{2+}$ release events (maximum fluorescence to maximum fluorescence) were calculated before and after addition of $H_2O_2$. Images were taken once per second (excitation Fluo4: 490 nm, emission 510 nm, exposure: 100 ms, ***p<0.001 with n=8 from three independent experiments (t-test)).*

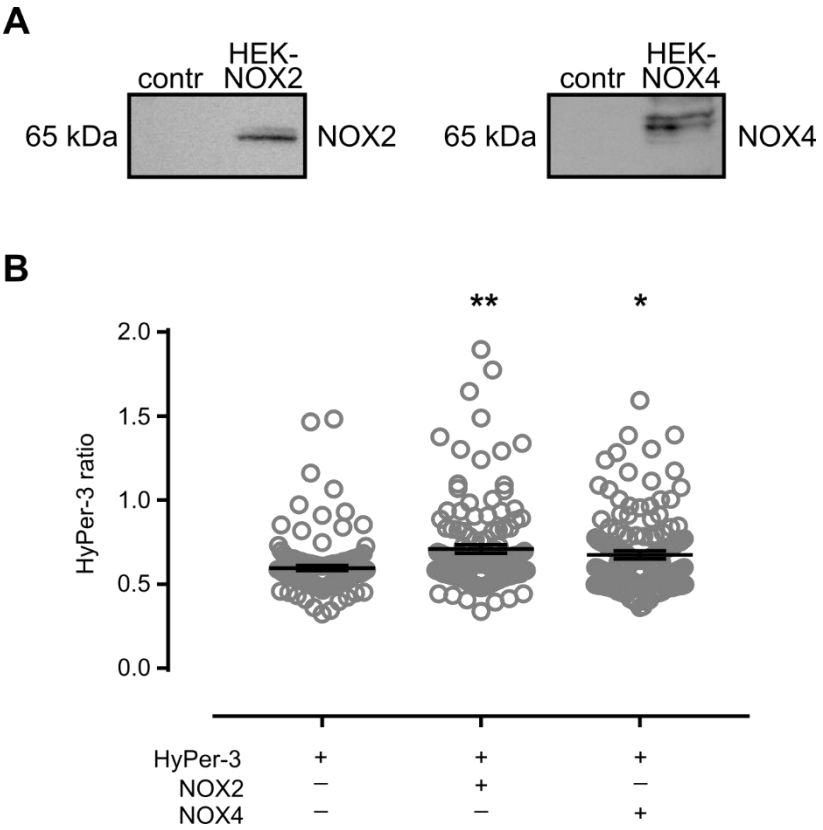


***Figure 11: NOX-transfected HEK293A cells show elevated levels of ROS.***

*HEK293A cells were co-transfected with HyPer-3 and NOX2 or NOX4, or with HyPer-3 alone. Cells were either harvested for Western blot analysis* ***(A)*** *or imaged for ROS monitoring* ***(B).*** *Cells were incubated in Tyrode's solution (1.8 mM $Ca^{2+}$). Multiple areas in one microscopy dish were imaged. Background-subtracted HyPer-3 ratios were calculated for single HyPer-3 and double-transfected HyPer-3/NOX cells (n≥ 134, **p>0.01, *p>0.05 (ANOVA)).*

## 3.3. Characterization of subcellular localization of NOX4 in ventricular cardiomyocytes

In parallel to the HEK293A cell model, the subcellular localization of NOX4 and its potential regulatory impact on RyR2 channel function was investigated in a ventricular cardiomyocyte environment. As NOX4 expression in ventricular cardiomyocytes is elevated in pathophysiological conditions, an adenoviral transduction vector (Ad5.NOX4) was designed to increase NOX4 expression in isolated ventricular cardiomyocytes from wt mice.

In a first step, short-term cultivation of ventricular cardiomyocytes (VMs) was established. After isolation of VMs using a Langendorff perfusion setup (see 2.2.1.2), cells were re-introduced stepwise to $Ca^{2+}$ and cultivated in culture medium for up to 48 h (see 2.2.1.3). Characteristics of functional intact cells (i.e., rod-shaped cell morphology, cross striations) were confirmed at 24 h and 48 h after isolation by light microscopy (Figure 12).

Next, cultivated cells were inoculated with different concentrations of an eGFP control virus (Ad5.eGFP) to titrate the multiplicity of infection (MOI) necessary for a high transduction efficiency. After 48 h of viral transduction, an MOI of 500 resulted in a transduction efficiency ≥ 75 % while maintaining characteristics of intact cells (Figure 13).

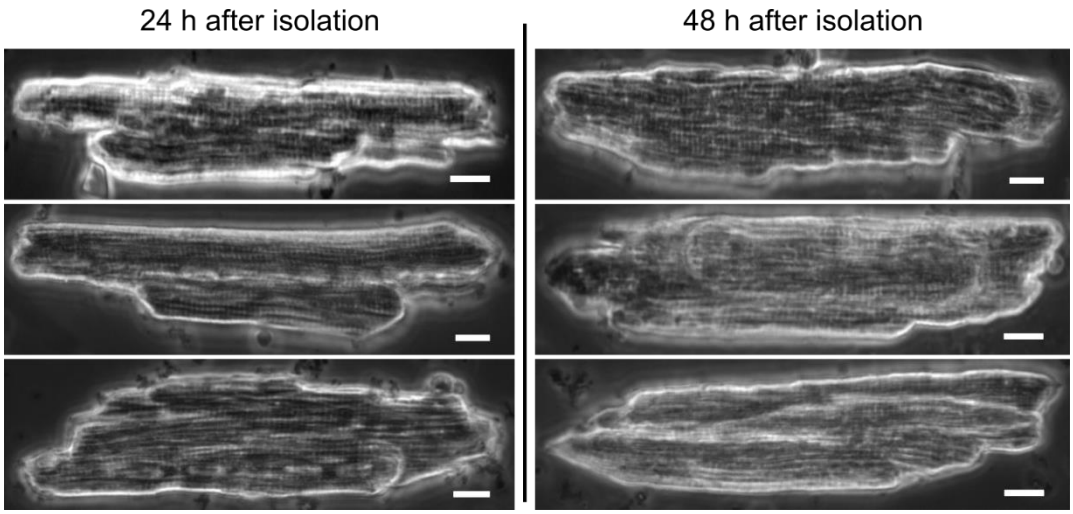


***Figure 12: Isolated ventricular cardiomyocytes could be cultivated for up to 48h.***
*Ventricular cardiomyocytes were isolated using collagenase type II and Langendorff perfusion. After isolation, cells were stepwise re-introduced to $Ca^{2+}$ and cultivated in culture medium (T. O'Connell et al., Isolation and Culture of Adult Mouse Cardiac Myocytes for Signaling Studies, 2003). Scale bar = 10 µm.*

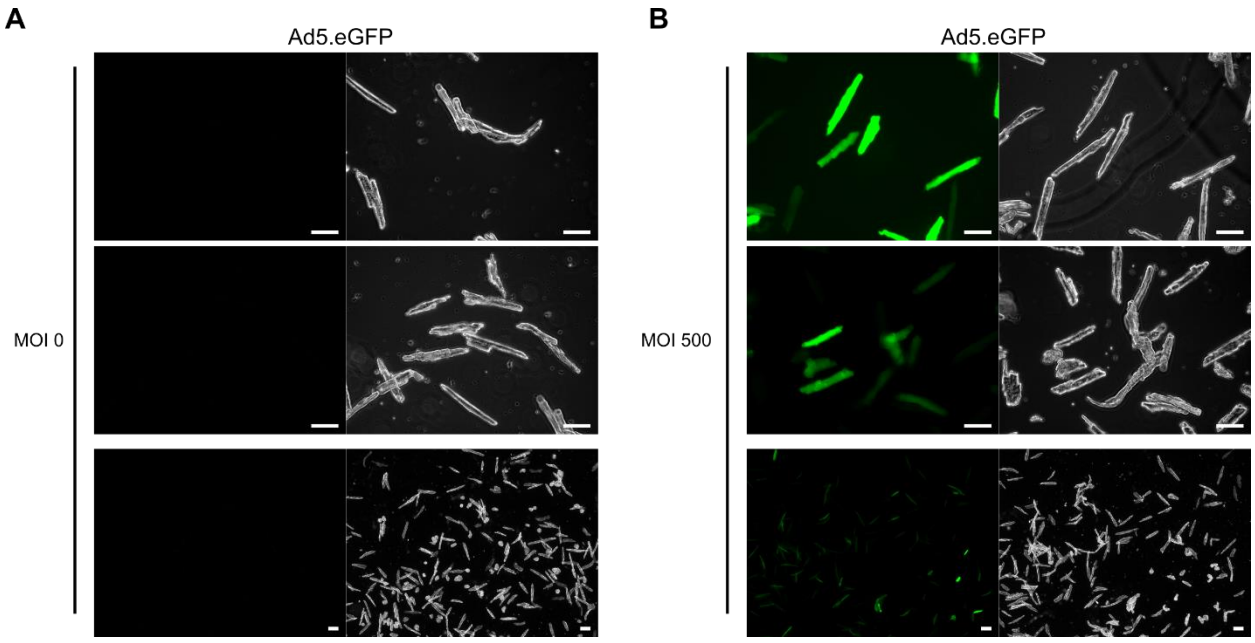


***Figure 13: Viral particle titration for transduction of cultured cardiomyocytes.***

*Ventricular cardiomyocytes were isolated as described earlier. Myocytes were inoculated with an eGFP expressing control virus (Ad5-eGFP) and incubated for 48 h. Different multiplicities of infection (MOI) were tested for optimization of transfection efficiency and cell viability. A MOI of 500 was sufficient for a transfection efficiency ≥ 75 % while maintaining characteristics of intact cells. Scale bar = 50 µm*

To confirm elevated levels of NOX4 expression in Ad5.NOX4-transduced ventricular cardiomyocytes, Western blot analysis was performed (Figure 14). Inoculation with Ad5.NOX4-viral particles at MOIs of 500 and 1000 clearly induced expression of NOX4. An MOI of 500 was used for all further experiments, as a MOI of 1000 was not sufficient to increase NOX4 expression compared to an MOI of 500.

For investigation of the subcellular localization of NOX4, virally transduced ventricular cardiomyocytes were subjected to immunocytochemistry. In short, ventricular cardiomyocytes from wt mice were isolated and subjected to short-term cultivation. Shortly after isolation, the cells were inoculated with either Ad5.NOX4 or Ad5.eGFP as a control. Following 48 h of viral

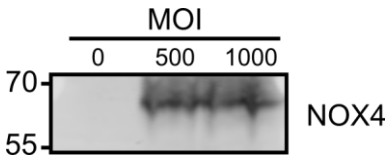


***Figure 14: Viral transfection of cultured cardiomyocytes induces NOX4 expression.***

*Western blot analysis of NOX4 expression levels in ventricular cardiomyocytes transduced with different MOIs of the Ad5.NOX4 virus shows a clear induction of NOX4 expression with an MOI of 500 and 1000 compared to control (MOI=0).*

transduction, cells were fixed using 4 % PFA and incubated with primary antibodies against NOX4 and RyR2. After washing and incubation with suitable secondary antibodies, cells were subjected to fluorescence microscopy (Figure 15). Confocal imaging revealed that NOX4-expression was clearly increased as indicated by an increase of NOX4 fluorescence signals in different parts of the cell in Ad5.NOX4 VMs (Figure 15A) compared to Ad5.eGFP-transduced control cells (Figure 15B). Superresolution STED nanoscopy demonstrated numerous punctate signal clusters for NOX4 (red) (Figure 15C), of which a fraction showed overlap with RyR2 (green) signal clusters, visualized by a line profile (Figure 15D). For quantification of overlapping clusters, fluorescence

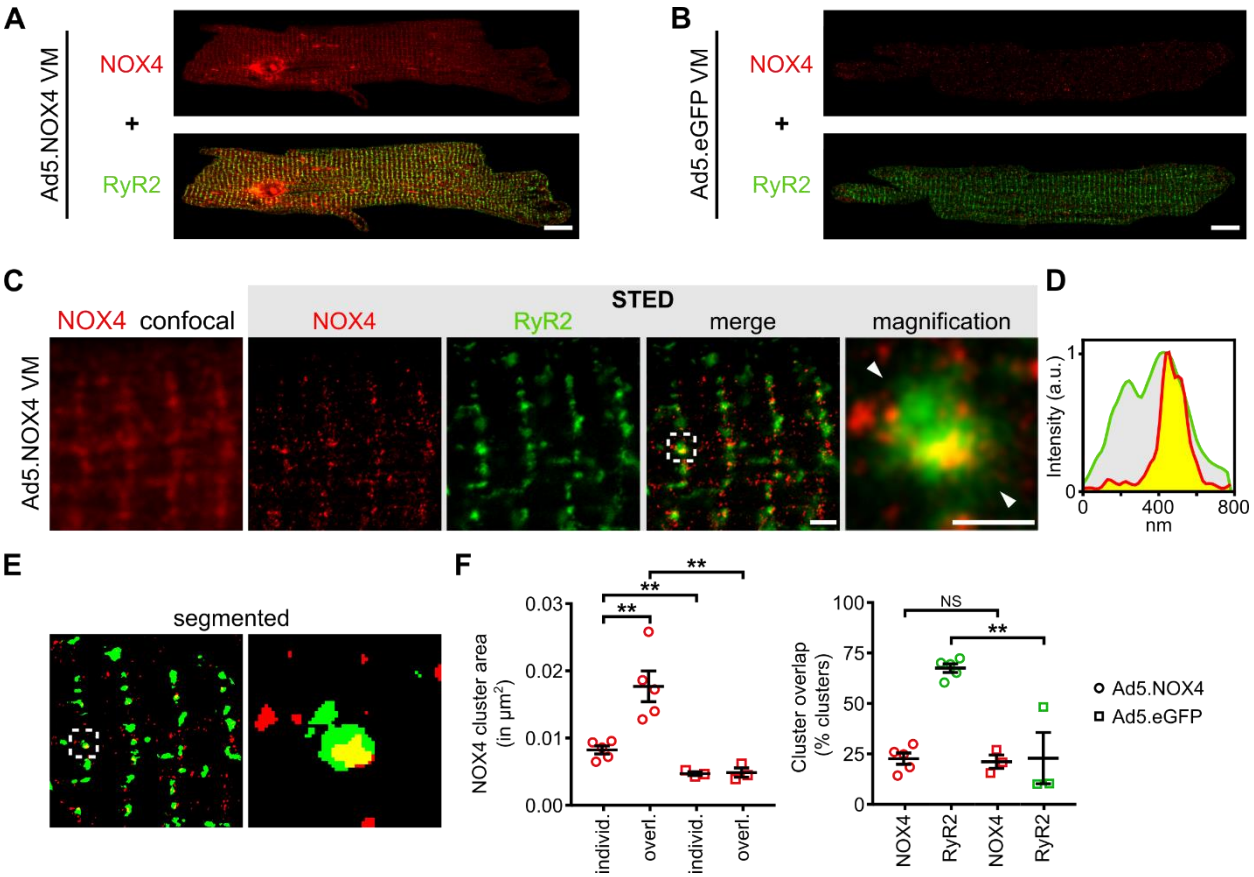


***Figure 15: Confocal and STED microscopy shows overlapping clusters of NOX4 and RyR2 in virally transduced myocytes.***

*Ventricular cardiomyocytes from wt mice (B6N, female, 17 weeks) were isolated and cultivated for 48 h. Shortly after isolation, myocytes were inoculated with either Ad5.NOX4* ***(A)*** *or Ad5.eGFP (MOI 500)* ***(B)*** *(scale bar = 10 µm). For immunocytochemistry, cells were stained for NOX4 and RyR2 and samples were subjected to STED nanoscopy.* ***(C)*** *STED superresolution nanoscopy reveals overlap of NOX4 and RyR2 fluorescence signals, visualized in a line profile of fluorescence intensities* ***(D)*** *(scale bar: merge = 1 µm; magnification = 400 nm).* ***(E)*** *For segmentation of NOX4 and RyR2 signals, images were background subtracted and thresholded (NOX4: local threshold (MidGrey); RyR2: local threshold (Bernsen)).* ***(F)*** *ImageJ was used to calculate cluster size and cluster overlap. Prism was used for statistical analyses (n≥3, **: p<0.01 (t-test))*

signals for NOX4 and RyR2 were segmented. For that, STED images were background subtracted and thresholding algorithms were applied (for NOX4: local thresholding (MidGrey); for RyR2: local thresholding (Bernsen)) (Figure 15E). Segmented images were then used to calculate cluster sizes of NOX4 and RyR2 signal clusters and percentage of overlapping NOX4/RyR2 signal clusters (Figure 15F). In Ad5.NOX4 VMs cluster size of NOX4 overlapping with RyR2 was significantly increased compared to individual, i.e., non-overlapping, NOX4 clusters ((0.01769 $\mu m^2$ ± 0.0023 (overlapping clusters) vs. 0.00824 $\mu m^2$ ± 0.0006 (individual clusters) n≥3, p<0.01 (t-test).). However, individual NOX4 cluster size in Ad5.NOX4 VMs was still significantly larger compared to NOX4 clusters in Ad5.eGFP VMs (0.00824 $\mu m^2$ ± 0.0006 (Ad5.NOX4) vs. 0.00472 $\mu m^2$ ± 0.0007 (Ad5.eGFP)). Additionally, RyR2 signal clusters overlapped significantly more frequently with NOX4 signal clusters in Ad5.NOX4 VMs compared to control cells (67.5% ± 2.1 (Ad5-NOX4) vs. 22.9% ± 12.7 (Ad5-eGFP), n≥3, p<0.01 (t-test)).

As immunocytochemistry revealed a close spatial association of NOX4 and RyR2 in VMs, a co-immunoprecipitation assay was performed to assess whether this association is facilitated via a direct or indirect protein-protein interaction. For that, Ad5.NOX4-transduced ventricular cardiomyocytes were lysed and incubated with a FLAG-antibody targeted against the C-terminal FLAG-tag of the transduced NOX4. Following the same protocol as co-immunoprecipitation assays in transfected HEK293A cells (see above), precipitated proteins were subjected to SDS-PAGE and Western blot analysis. Here, endogenous RyR2 was co-purified with NOX4 (Figure 16).

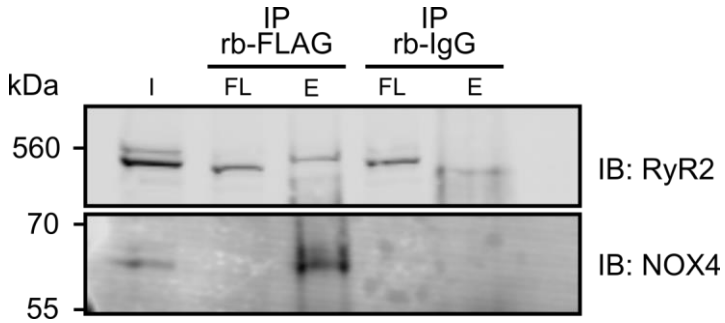


***Figure 16: RyR2 co-immunoprecipitation with NOX4 in ventricular cardiomyocytes.***

*Isolated ventricular cardiomyocytes transduced with Ad5.NOX4 were lysed and subjected to co-immunoprecipitation analysis. Immunoprecipitation of NOX4 via its FLAG-tag resulted in co-elution of RyR2 (IP= immunoprecipitation, I= Input, FL= Flow-through, IB= Immunoblot).*

## 3.4. Identification of redox-sensitive RyR2 cysteine residues

As oxidative regulation of proteins is often facilitated by redox-dependent modifications of certain cysteine residues, an approach for the identification of redox-sensitive cysteine residues in RyR2 was developed. First described by *Anjo et al.*, an experimental strategy termed oxSWATH combines differential alkylation of a sample and its subsequent analysis by data-independent mass spectrometry (Figure 17) [119]. In a first step, reduced cysteine residues in a biological sample are blocked by an alkylating agent, for example iodoacetamide (IAM). The sample is then reduced either with an unspecific reductant (e.g. tris(2-carboxyethyl)phosphine (TCEP)) or with a modification-specific reductant (e.g. ascorbic acid for S-nitrosylated cysteine residues). In a second alkylation step, the now reduced cysteines are blocked by a second alkylating agent (e.g., N-Ethylmaleimide (NEM)), which can be discriminated from the first alkylating agent by mass spectrometry. After digestion of the proteins, the peptides are analyzed using data-independent

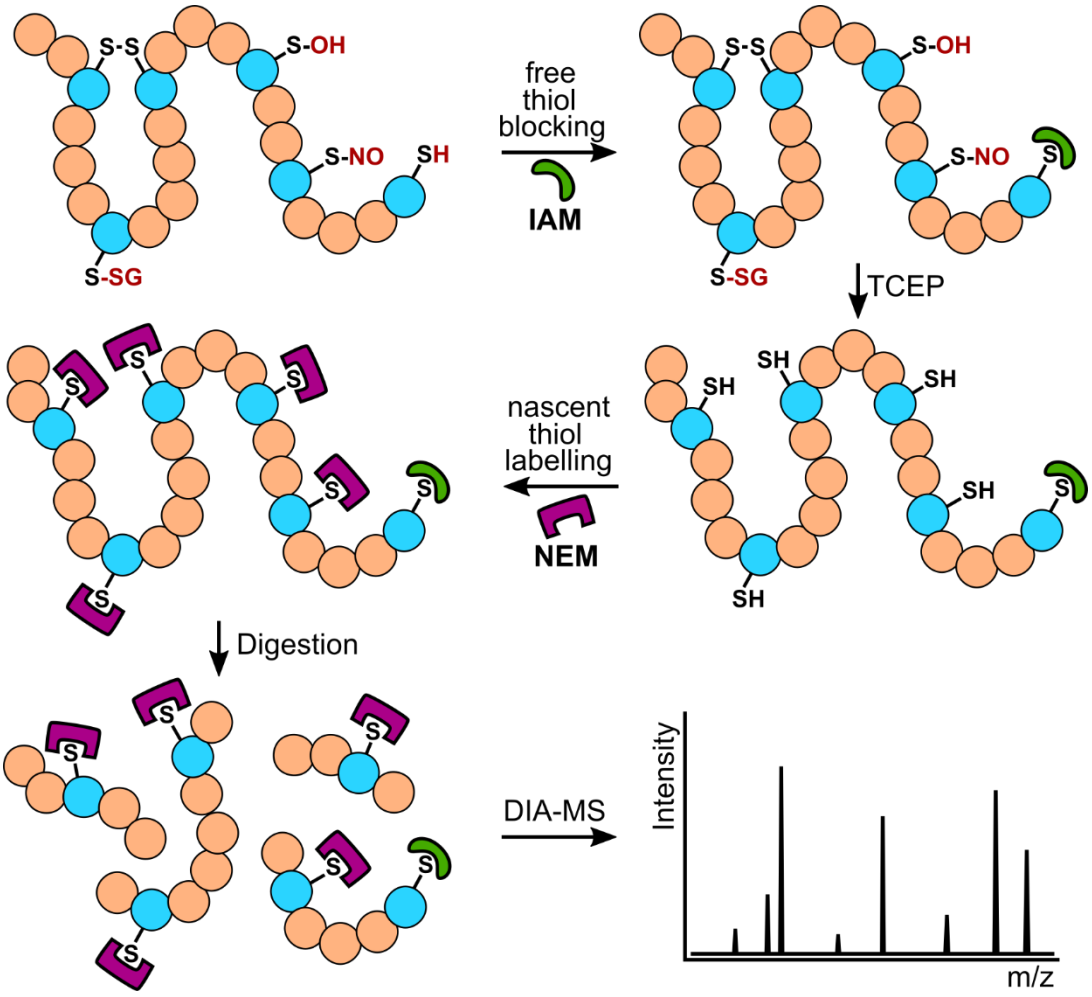


***Figure 17: Schematic overview of the oxSWATH workflow.***

*Detailed explanation in the text. Adapted from S. Anjo et al.*

mass spectrometry. All in all, oxSWATH is able to identify individual redox-sensitive cysteine residues in a target protein.

First experiments were performed to establish this workflow (2.2.2.5). To test alkylation efficiency, HEK293A cell lysate was incubated with the alkylating agent biotin-maleimide (Bt-maleimide) (Figure 18A). This alkylation was visualized by Western blot analysis using a fluorophore-linked Streptavidin. In this analysis, a strong signal on the blot corresponded with a high degree of cysteine alkylation by Bt-maleimide. Prior incubation of HEK293A cell lysates with NEM or

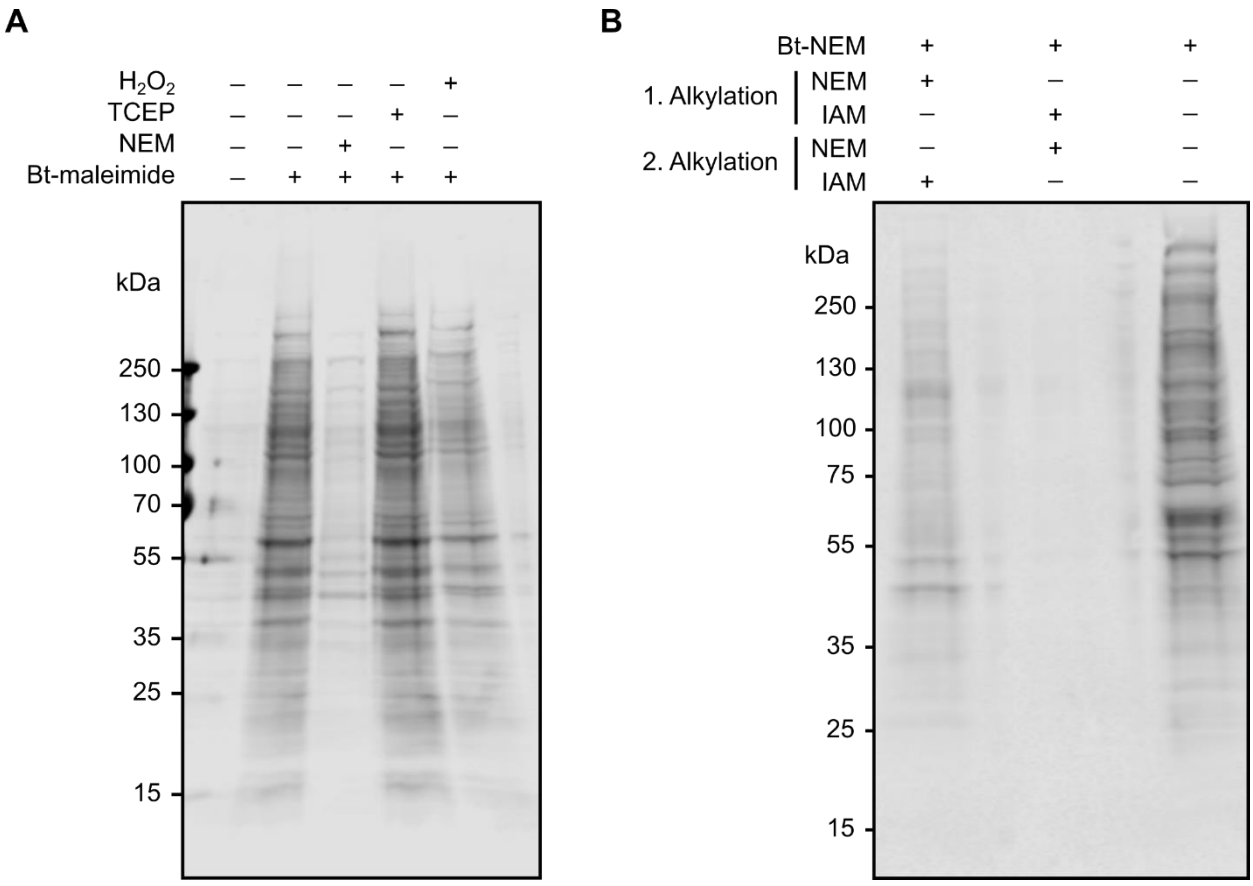


***Figure 18: Cysteine thiol alkylation in HEK293A cells.***

*Cell lysate of HEK293A cells was used to establish an alkylation protocol.* ***A)*** *HEK293 cell lysates were oxidized ($H_2O_2$, 1 mM), reduced (TCEP, 10 mM) or alkylated (NEM, 10 mM) before treatment with biotin-labeled maleimide (Bt-maleimide, 10 mM) to test alkylation efficiency. Prior incubation of samples with NEM or oxidation by $H_2O_2$ reduces biotin-maleimide alkylation.* ***B)*** *Iodoacetamide (IAM) and N-ethylmaleimide (NEM) were used for sequential alkylation. HEK293 cell lysates were either incubated with IAM (66 mM) or NEM (10 mM). After removing the first alkylating agent by using a 5 kDa cut-off filter, samples were reduced by addition of 10 mM TCEP. After incubation with the according second alkylating agent (NEM: 10 mM; IAM: 66 mM), biotin-maleimide was added and samples were subjected to Western blot analysis. The sequential alkylation decreased alkylation by biotin-maleimide, especially if IAM was used as the first alkylating agent.*

oxidation with $H_2O_2$ decreased Bt-maleimide alkylation, while prior reduction of samples with TCEP did not change alkylation efficiency.

To test if the order of alkylation in a sequential alkylation protocol impacts overall alkylation efficiency, HEK293A cells were initially incubated with either NEM or IAM (Figure 18B). After removal of the alkylating agent by using a 5 kDa cut-off centrifugation filter, lysates were reduced by TCEP and alternatingly incubated with either IAM or NEM, respectively. Lysates were finally incubated with Bt-maleimide to visualize alkylation efficiency by Western blot analysis. Bt-maleimide alkylation was reduced by both orders of sequential alkylation, especially when IAM was used as the first alkylating agent.

To investigate if viral induction of NOX4 expression impacts the overall redox-status of cysteine residues in ventricular myocytes, alkylation was tested using lysates of either Ad5.eGFP- or Ad5.NOX4-transduced VMs (Figure 19). Ventricular cardiomyocytes from wt mice were isolated

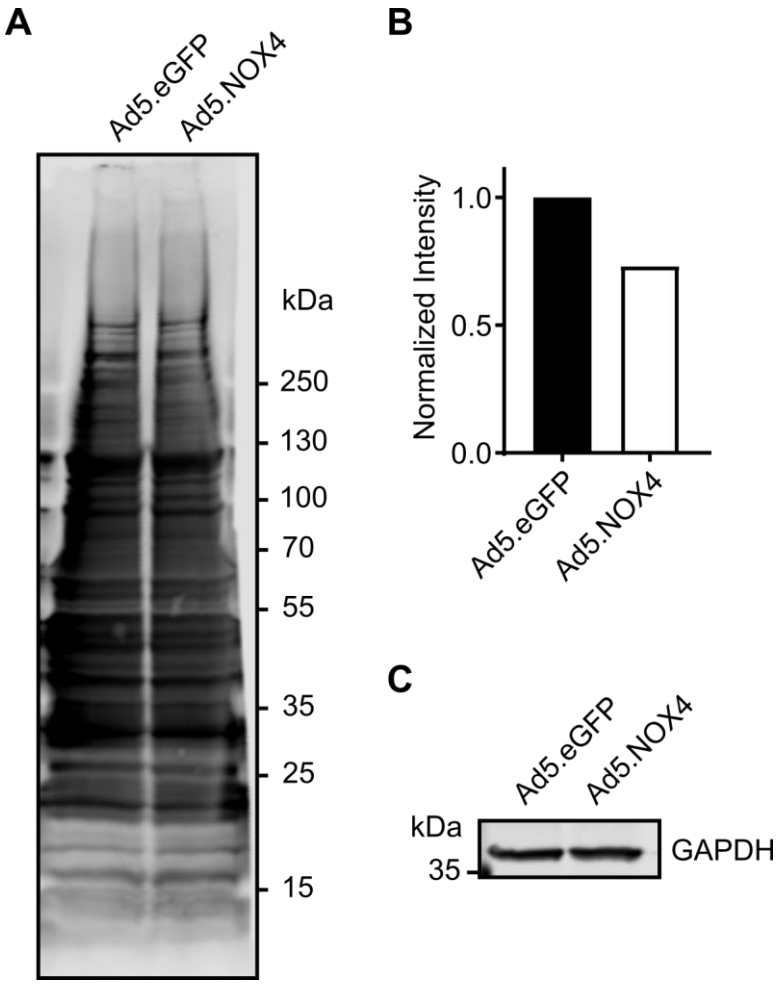


***Figure 19: Alkylation of cysteine thiols in virally transduced myocytes.***

*Lysates from isolated ventricular cardiomyocytes (transduced with either Ad5.eGFP or Ad5.NOX4) were alkylated with biotin-maleimide (10 mM).* ***A****) A streptavidin-linked fluorescent antibody was used to detect the biotin after Western blot.* ***C)*** *GAPDH was used for signal intensity normalization.* ***B)*** *Signal intensity is decreased in myocytes transduced with Ad5.NOX4, compared to Ad.5eGFP-transduced control cells.*

and virally transduced as described above (2.2.1.4). After harvesting and lysis of the myocytes, lysates were incubated with Bt-maleimide. Western blot analysis revealed that alkylation with Bt-maleimide was decreased in Ad5.NOX4-transduced VMs compared to Ad5.eGFP control cells (Figure 19B). GAPDH was used as a loading control for quantification and was used to normalize and thus compare Bt-maleimide signals (Figure 19C).

In summary, the results presented in this thesis depict the establishment of a HEK293A cell model for the analysis of modulations of RyR2 channel activation. Further, superresolution STED microscopy revealed a close association of NOX4 and RyR2 at sarcoplasmic reticulum membranes in virally transduced cardiomyocytes. Finally, foundational experiments for the identification of RyR2-specific cysteines that are modulated by NOX-dependent ROS production were performed, thus providing the groundwork for further mass-spectrometry-based analyses.

# 4. Discussion

Cardiomyocyte function is dependent on a well-coordinated calcium release from the sarcoplasmic reticulum. This release is facilitated by clusters of RyR2 calcium channels within the SR membrane. Tight regulation of RyR2 channel activity is therefore of crucial importance for cardiomyocyte function and involves numerous post-translational modifications such as phosphorylation. While redox-dependent modifications of RyR2 are known, their mechanisms and consequences are not yet fully understood. The NADPH-dependent oxidases NOX2 and NOX4 have been shown to be involved in the regulation of the calcium homeostasis in cardiac and skeletal muscle cells. It is therefore hypothesized that NOX2 and NOX4 act as potential regulators of RyR2 channel activity by specific production of ROS and thus RyR2 oxidation in cardiomyocytes.

This study was designed to explore the impact of NOX-dependent ROS production on RyR2 channel activity. For that purpose, essential steps in the generation of a HEK293A model were achieved. Using live-cell epifluorescence microscopy, it was demonstrated that HEK293A cells transiently expressing human RyR2 (hRyR2) show spontaneous and periodic $Ca^{2+}$ release events. The frequency of these $Ca^{2+}$ release events could be increased by RyR2 oxidation via addition of exogenous $H_2O_2$. Additionally, NOX-expressing HEK293A cells feature a more oxidized cytosolic environment as indicated by ratiometric HyPer-3 fluorescence microscopy.

In parallel, superresolution STED nanoscopy was performed to investigate the subcellular localization of NOX4 in virally transduced isolated ventricular cardiomyocytes. Here, a colocalization analysis revealed a close association of NOX4 and RyR2 at the SR membrane. Further evaluation of this association by co-immunoprecipitation consolidated a direct protein interaction of NOX4 and RyR2.

As redox-dependent modifications of cysteine residues in RyR2 were shown to regulate RyR2 activity, a strategy combining differential cysteine residue alkylation and data-independent mass spectrometry was developed investigating specific cysteine residues of RyR2 that are potential targets for NOX-dependent redox modifications. Preparatory experiments using HEK293A cell lysates were performed and a protocol for the differential alkylation was established.

## 4.1. Functional ROS and $Ca^{2+}$ measurement in the HEK293A cell model

Previously introduced by Chen and colleagues [19,120,121], HEK293A cells expressing RyR2 have repeatedly been used to study RyR2 channel function. Consistent with the literature, HEK293A cells transiently expressing hRyR2, as presented in this thesis, exhibited spontaneous and periodic $Ca^{2+}$ release events (see Figure 9). The RyR2-binding compound ryanodine was used

to ensure that the observed $Ca^{2+}$ release is a direct consequence of RyR2 expression. While nanomolar concentrations of ryanodine retain the RyR2 channel in its open state, the micromolar concentration used here fully inhibits RyR2 channel activity [122]. These findings indicate that the $Ca^{2+}$ release in transfected HEK293A cells is indeed RyR2-mediated, which is also in line with prior publications [19,120].

Comparing the characteristics of the RyR2-mediated $Ca^{2+}$ release in HEK293 cells with those in cardiomyocytes, there are clear distinctions regarding the general dynamic of the process. Concerning this matter, it needs to be addressed that the mechanisms involved in the spontaneous $Ca^{2+}$ release by RyR2 in HEK293A cells are only incompletely understood. Some literature suggests the concept of "store-overload induced $Ca^{2+}$ release" (SOICR) to be causative for RyR2 activation and thus $Ca^{2+}$ release from the endoplasmic reticulum [120,123]. According to this concept, RyR2 channels are directly activated once a certain endoplasmic calcium concentration is reached. However, it is debated to which extent this concept is relevant for the physiological calcium homeostasis in cardiac muscle cells [124].

It can certainly be assumed that RyR2 channel activity in the HEK293A model differs from that in cardiomyocytes for several reasons: As demonstrated by superresolution STED nanoscopy (Figure 7B), RyR2 clusters are distinctly smaller in HEK293A cells compared to cluster sizes in cardiomyocytes [16]. Cluster size and the resulting organization of RyR2 molecules within a cluster are increasingly recognized as crucial characteristics for RyR2 channel activity in cardiomyocytes [125]. A reductionist approach, the HEK293A cell model does not include proteins that are physiologically involved in RyR2 regulation (e.g., FKBP12.6, calmodulin, etc.). However, live-cell epifluorescence imaging before and after the addition of hydrogen peroxide (Figure 10) demonstrated that RyR2 channel activity can still be modulated by oxidation, which corroborates previous results (*Waddell et al.*, 2016) [123]. Taking into account the limitations discussed above, RyR2-expressing HEK293A cells represent a useful model system for investigating the potential regulatory impact of NOX-dependent ROS production on RyR2 channel activity.

HEK293A cells transfected with NOX2 or NOX4 exhibited significantly elevated levels of ROS, indicated by a increasingly oxidized fluorescent $H_2O_2$-probe HyPer-3 (Figure 11). Notably, this increase in cytosolic ROS production was already apparent without the need for further stimulation or NOX activation. HEK293A cells have previously been described to express the NOX isoforms NOX1 and NOX2 and their respective cytosolic regulatory subunits [126]. As transfection of HEK293A cells with both NOX isoforms induced expression of p22phox as demonstrated by Western blot analysis (Figure 6A) and NOX-mediated ROS production depends on complex formation with p22phox, the increase in ROS levels observed here is likely caused by an increase in enzymatically active NOX complexes.

A cloning strategy was developed to combine NOX2 or NOX4 and the $H_2O_2$ probe HyPer-3 into one single expression plasmid to overcome low transfection efficiencies, especially in double-

transfected HEK293A cells (see Appendix Figure 20). Using pBudCE4.1 as the vector backbone, both the respective NOX isoform and HyPer-3 are co-expressed individually. This additionally serves as a transfection control, as HyPer-3-expressing cells, that can clearly be distinguished from non-transfected cells by fluorescence microscopy, also express either NOX2 or NOX4.
Summarizing, the results discussed thus far depict fundamental steps in establishing a HEK293A cell model that can be utilized for further investigation of the potential regulatory impact of NOX-dependent ROS production on RyR2 channel activity.

### 4.1.1. Future perspectives

The use of HEK293A cells expressing RyR2 and the cardiac NOX isoforms NOX2 and NOX4 provides a potent model system to investigate a direct regulation of RyR2 channel activity by NOX-generated ROS. While recognizing the distinct differences to cardiomyocytes, this model offers specific advantages regarding flexibility, reproducibility and manipulability.
As a heterologous expression system, it focuses on the source of ROS production (NOX) and its potential target (RyR2). Modulation of NOX activity monitored by HyPer-3 fluorescence can be applied to examine if an increase or decrease in NOX-dependent ROS production directly impacts RyR2 channel activity, thereby emphasizing the specificity of this regulation. With regard to NOX inhibition, several compounds such as diphenylene iodonium (DPI) or the NOX2-specific blocking peptide tat-gp91ds have been described and critically discussed in the literature [127]. The recently discovered X-ROS signaling pathway in cardiomyocytes gives valuable insights into NOX2-dependent ROS production and its impact on RyR2 channel activity [108]. There, mechanical activation of NOX2 by stretching of cardiomyocytes results in increased activation of RyR2 channels. This signaling pathway could be interrupted by addition of the NOX2-specific inhibitor tat-gp-91ds [128]. As detailed mechanisms and potentially involved compounds of this NOX2/RyR2 interaction are yet to be fully understood, the model presented here may help to inform whether RyR2 channel activity is directly regulated by NOX or if other components in this signaling pathway are required.
Noteworthy, the effects of the NOX-dependent oxidation of RyR2 are possibly manifested in an altered interaction of RyR2 with further regulatory proteins only present in cardiomyocytes.
The inclusion of a luminal $Ca^{2+}$-sensitive dye, such as D1ER or its derivatives [129,130], to monitor endoplasmic calcium concentrations could also be an important addition to the model. This might help to clarify whether the oxidation of RyR2 by NOX results in a changed sensitivity of RyR2 to luminal $Ca^{2+}$.
Lastly, this model can be utilized for the functional characterization of specific redox-sensitive cysteine residues of RyR2. Once redox-sensitive cysteines have been identified, RyR2 mutants lacking these cysteines can be introduced in the HEK293A model and investigated regarding their NOX-dependent regulation.

## 4.2. Subcellular localization of NOX4 and possible interaction with RyR2

A distinct subcellular localization of NOX2 and NOX4 in cardiomyocytes likely has a direct impact on their regulatory role, as the localization in different subcellular compartments brings the NOX isoforms into close proximity to potential targets for oxidation. While NOX2 has been predominantly associated to be expressed at the sarcolemma of cardiomyocytes [102], the exact subcellular localization of NOX4 is controversially discussed, as expression has been reported in the nucleus, in mitochondria or at the endoplasmic reticulum membrane [95,105,131]. Cell-type specific localization and expression of NOX4 splice variants have been made responsible for these findings. In cardiomyocytes, a sarcoplasmic localization has been proposed [109]. To further investigate NOX4 localization and its potential relation to RyR2, superresolution STED nanoscopy was performed in NOX4 and hRyR2 co-transfected HEK293A cells and Ad5.NOX4-transduced mouse ventricular cardiomyocytes.

STED nanoscopy in HEK293A cells expressing NOX4 and RyR2 revealed a close spatial proximity of both proteins at the ER membrane (Figure 7). Since this indicated a potential protein-protein interaction, a co-immunoprecipitation protocol was developed. Here, RyR2 was co-purified with NOX4 in double-transfected HEK293A cells, indicating a direct interaction. For co-immunoprecipitation, the choice of suitable controls is crucially important, as it determines the specificity of any detected protein interaction. For that, HEK293A cells were additionally transfected with JPH2, which was co-purified with RyR2 but not with NOX4. As the interaction of JPH2 and RyR2 in cardiomyocytes is well characterized [16,118], the confirmed interaction here served as a positive control for the co-immunoprecipitation protocol. The fact that JPH2 was not co-purified with NOX4 while preserving the interaction of NOX4 and RyR2 simultaneously excludes potential false-positive results since there is no known interaction of JPH2 and NOX4.

The use of a heterologous expression system for protein-protein interaction studies requires certain limitations to be considered. Transient transfection can induce cell stress as it circumvents normal cellular regulatory mechanisms for protein expression. This results in the desired overexpression of the target proteins, but could also introduce overexpression artifacts such as protein misallocations, since exogenous proteins might lack important cell type-specific interaction partners for proper trafficking [132,133]. To address these limitations, an adenoviral vector was designed to induce moderate expression of NOX4 in their native ventricular cardiomyocyte environment to further investigate NOX4 localization and the potential interaction with RyR2. This was also necessary, as endogenous NOX4 expression levels in ventricular cardiomyocytes were very low and thus unsuitable for further analyses.

A published protocol (*O'Connell et al.*, 2007) was adapted for the isolation and cultivation of ventricular cardiomyocytes (Figure 12) [134]. To maintain cell quality and viability during viral transduction and to prevent an excess of NOX4 expression, the MOI was carefully titrated. An

MOI of 500 was sufficient for induction of moderate NOX4 overexpression in >75% of cells and simultaneous preservation of cell viability (Figure 13 and Figure 14).

Superresolution STED nanoscopy of Ad5.NOX4-transduced cardiomyocytes revealed a close association of NOX4 and RyR2 signals with partially overlapping fluorescence signaling clusters (Figure 15). This strongly suggests a sarcoplasmic localization of NOX4 in ventricular cardiomyocyte, corroborating previous speculations [95,115]. A cluster analysis of NOX4 and RyR2 signals demonstrated that NOX4 clusters that overlap with RyR2 clusters are significantly larger in regard to cluster area compared to non-overlapping NOX4 clusters. Moreover, significantly more RyR2 clusters showed an overlap with NOX4 clusters in Ad5.NOX4-transduced cardiomyocytes compared to Ad5.eGFP-transduced control cells. This emphasizes that the observed close association of NOX4 and RyR2 in cardiomyocytes might be the result of a physiologically meaningful complex formation. Of note, fluorescence microscopy also showed a perinuclear or nuclear NOX4 signal. A perinuclear accumulation of NOX4 could be caused by the increase of NOX4 protein biosynthesis due to the viral transduction. As stated above, it has been speculated that NOX4 also locates to the nucleus. However, only the 28 kDa splice variant NOX4D was identified in the nucleus of vascular smooth muscle cells thus far [106]. When working with antibodies for specific detection of target proteins, eventually, it is a common phenomenon that antibodies can present unspecific signals or cross-reactions with non-target proteins [135]. Therefore, it remains to be further investigated whether the virally transduced full-length NOX4 used in this thesis is also able to localize to the nucleus.

While STED nanoscopy greatly increases spatial resolution of individual fluorescence signals and minimizes unspecific background, an overlap of fluorescence signals is only an indication of a possible protein-protein interaction and needs to be validated by complementary experiments. To further validate if the observed close association of NOX4 and RyR2 is a consequence of a direct protein interaction, a co-immunoprecipitation assay following the protocol established for the transfected HEK293A cell model was performed in virally transduced cardiomyocytes. In line with the identified NOX4/RyR2 interaction in HEK293A cells, this interaction could also be confirmed in ventricular cardiomyocyte lysates (Figure 16).

While this novel interaction of NOX4 and RyR2 in cardiomyocytes has been demonstrated in this thesis for the first time, a similar interaction of NOX4 with the skeletal muscle isoform RyR1 has been described [110]. There, NOX4 directly increases RyR1 activity by ROS-generation and subsequent oxidation of RyR1 cysteine thiols. As this regulation of RyR1 by NOX4 was found to be dependent on partial oxygen pressure ($pO_2$), it has been theorized that NOX4 acts as an oxygen-dependent regulator of RyR1-mediated $Ca^{2+}$ release. It is conceivable that the NOX4-RyR2 interaction in cardiomyocytes represents a $pO_2$-coupled regulation of $Ca^{2+}$ release in a similar fashion.

Taken together, these results offer vital evidence for the hypothesis that NOX4 and RyR2 colocalize at the SR membrane to potentially form a complex for the regulation of RyR2 channel activity.

## 4.3. Identification of ROS-sensitive RyR2 cysteines

For a better understanding of the detailed mechanisms of RyR2 oxidation by NOX-generated ROS, it is of paramount importance to identify specific cysteine residues as target for these redox-dependent modifications. While general ROS-sensitive cysteines have been identified for RyR1, significantly less is known for RyR2 [63]. Knowing these cysteines can guide further research to elucidate e.g., NOX isoform-specific targets in RyR2.

For the identification of ROS-sensitive RyR2 cysteines that are modified by NOX-generated ROS, initial experiments were performed, following a protocol recently published by Anjo et al. termed oxSWATH, which combines differential alkylation and data-independent mass spectrometry [119]. In this approach, the differential alkylation of redox-modified cysteine residues is crucial to transform labile and transient cysteine oxidations into stable and detectable cysteine alkylations, which can subsequently be analyzed by mass spectrometry. Thus, the redox state and general expression levels of proteins of interest can be evaluated simultaneously. For that, an alkylation protocol using NEM and IAM was successfully established using HEK293A wt cell lysate, showing a high degree of cysteine alkylation (Figure 18). As sequential alkylation with IAM as the first alkylating agent and NEM as the second one proved to be the most efficient in regard to total alkylation, all subsequent experiments were performed following that protocol.

The differential alkylation protocol was applied to Ad5.NOX4-transduced isolated cardiomyocytes to examine the impact of NOX4-dependent ROS production on the redox status of RyR2 cysteines. A first analysis by data-independent mass spectrometry will be performed in future experiments.

A comparison of biotin-maleimide-alkylated lysates from Ad5.eGFP vs. Ad5.NOX4-transduced cardiomyocytes revealed an overall decreased level of reduced cysteine thiols in Ad5.NOX4-transduced cells (Figure 19). This could be a direct consequence of an increase in NOX4-dependent ROS production. As this was only one single experiment, further validation of this finding needs to be done.

While oxidation-dependent modifications of RyR2 in the cardiomyocyte context as mentioned in 1.3 have been highlighted in the literature as a major factor for cardiomyocyte function in (patho)physiological conditions, the impact of redox dependent posttranslational modifications of RyR2 channels in other tissues is increasingly subject of other fields of research. RyR2 oxidation has, for example, been described to be involved in the progression of Huntington's Disease (HD), which is characterized by neurodegeneration, but also pulmonary and cardiac dysfunction [136]. In

all involved tissues, RyR2 oxidation might pose as a potential therapeutic target and elucidation of specific targets for oxidation in RyR2 could help to better understand (patho)physiological mechanisms.
In summary, a differential alkylation protocol was established as a fundamental step for the identification of redox-sensitive cysteine residues particularly of RyR2 but also in cardiomyocytes in general. First experiments indicated an overall increase in thiol oxidation in NOX4-transduced isolated cardiomyocytes.

## 4.4. Outlook

This study was designed to characterize the potentially regulatory role of NOX-dependent ROS production on RyR2 channel activity in cardiomyocytes. To this end, a HEK293A cell model transiently expressing either NOX2/NOX4 or RyR2 was developed. This model demonstrated that RyR2 channel activity could be modulated by oxidation via addition of exogenous $H_2O_2$. Moreover, HEK293A cells expressing NOX2 or NOX4 showed elevated levels of ROS as measured by HyPer-3 fluorescence ratios. In future experiments, this model can be used to further investigate a direct oxidation of RyR2 by NOX2 or NOX4 and its impact on RyR2 channel activity. By STED nanoscopy of virally transduced isolated cardiomyocytes, in which NOX4 expression was elevated, it could be demonstrated that NOX4 is located at the SR membrane and was in close proximity with RyR2 channels. Subsequent co-immunoprecipitation assays revealed a direct protein interaction of NOX4 and RyR2, strongly implying a physiologically meaningful complex with potentially regulatory qualities. Functional calcium measurements in virally transduced cardiomyocytes are necessary to further evaluate the regulatory relationship of NOX4 and RyR2 by analyzing key characteristics of RyR2 channel function in future studies. Lastly, initial experiments were performed establishing a protocol for the differential alkylation of redox-modified cysteine residues in RyR2. This provides an experimental foundation for future studies to identify specific NOX-targeted cysteine residues in RyR2. These studies could include an analysis of potential NOX2- vs. NOX4-specific cysteines and additionally clarify the specific type of oxidative modification (e.g., glutathionylation, nitrosylation). Once specific cysteines are known, RyR2 mutants can be generated lacking these targets for NOX-specific oxidation. Channel function of these RyR2 mutants can be analyzed in complementary experiments using the established HEK293A cell model.
As a mass spectrometric analysis, the oxSWATH approach could furthermore be used to identify other targets of NOX-dependent oxidation besides RyR2, such as CaMKII, PKA or SERCA2a,

that have been discovered to be redox-modified and are potentially involved in pathophysiological processes [137].

The methods presented in this thesis lay the foundation for a further in-depth characterization of the regulatory impact of NOX-dependent ROS production on RyR2 channel activity. They can also be applied to provide a better understanding of the differential role of NOX2 and NOX4 in cardiomyocytes, especially in the context of (patho)physiological conditions such as exercise but also heart failure and cardiac hypertrophy [101,138]. While increased NOX2 activity has been identified as a pathogenic factor in the development of left ventricular hypertrophy, caused by an increased renin-angiotensin-aldosterone signaling or mediated via other GPCRs [139–142], elevated levels of NOX4 expression have been identified as beneficial in the context of chronic-load-induced cardiac stress [109]. The methods discussed here, can give valuable insight, whether these pathophysiological mechanisms involving NOX activation are mediated by RyR2 oxidation. Further, the identification of distinct, isoform-specific targets of NOX2 and NOX4 using the oxSWATH approach might provide a more complete understanding of consequences of NOX-dependent ROS production.

In future studies, the presented methods can also be complemented by additional techniques or cell models to address different effects of NOX activation or modulation on RyR2 activity. Since increased mitochondrial ROS production due to an elevation in cytosolic ROS is another major contributing factor to pathogenic mechanisms in heart failure, cardiomyocytes of transgenic mice expressing the mitochondrial redox sensor roGFP could be used for viral transduction experiments to assess the impact of NOX4- (or NOX2-) dependent ROS production on mitochondrial function [143]. The identification and characterization of specific redox events is also relevant for the development of new therapeutic interventions. Previous strategies involving the application of unspecific antioxidant agents to counteract conditions of increased oxidative stress have not proven to be effective, as they disregard the difference of physiological vs. pathological redox events.

In conclusion, the findings and methods presented in this thesis provide a fundamental groundwork for the elucidation of the importance of specific redox modifications in cardiomyocytes and their consequences for proper heart function.

## References


1. Hall, J. E. & Guyton, A. C. *Guyton and Hall Textbook of Medical Physiology*. (Saunders/Elsevier, 2011).
2. Camm, A. J., Lüscher, T. F., Serruys, P. W., & European Society of Cardiology. *The ESC textbook of cardiovascular medicine*. (Oxford University Press, 2009).
3. Fearnley, C. J., Roderick, H. L. & Bootman, M. D. Calcium Signaling in Cardiac Myocytes. *Cold Spring Harb. Perspect. Biol.* **3**, a004242 (2011).
4. Zima, A. V. & Mazurek, S. R. Functional Impact of Ryanodine Receptor Oxidation on Intracellular Calcium Regulation in the Heart. *Rev. Physiol. Biochem. Pharmacol.* **171**, 39–62 (2016).
5. Wang, S. Q., Song, L. S., Lakatta, E. G. & Cheng, H. Ca2+ signalling between single L-type Ca2+ channels and ryanodine receptors in heart cells. *Nature* **410**, 592–596 (2001).
6. Soeller, C. & Cannell, M. B. Examination of the transverse tubular system in living cardiac rat myocytes by 2-photon microscopy and digital image-processing techniques. *Circ. Res.* **84**, 266–275 (1999).
7. Fabiato, A. Calcium-induced release of calcium from the cardiac sarcoplasmic reticulum. *Am. J. Physiol.* **245**, C1-14 (1983).
8. Parmacek, M. S. & Solaro, R. J. Biology of the troponin complex in cardiac myocytes. *Prog. Cardiovasc. Dis.* **47**, 159–176 (2004).
9. Bassani, R. A., Bassani, J. W. & Bers, D. M. Mitochondrial and sarcolemmal Ca2+ transport reduce [Ca2+]i during caffeine contractures in rabbit cardiac myocytes. *J. Physiol.* **453**, 591–608 (1992).
10. Bassani, J. W., Bassani, R. A. & Bers, D. M. Relaxation in rabbit and rat cardiac cells: species-dependent differences in cellular mechanisms. *J. Physiol.* **476**, 279–293 (1994).
11. Shannon, T. R. & Bers, D. M. Integrated Ca2+ management in cardiac myocytes. *Ann. N. Y. Acad. Sci.* **1015**, 28–38 (2004).

12. Lanner, J. T., Georgiou, D. K., Joshi, A. D. & Hamilton, S. L. Ryanodine Receptors: Structure, Expression, Molecular Details, and Function in Calcium Release. *Cold Spring Harb. Perspect. Biol.* **2**, a003996 (2010).

13. Otsu, K. *et al.* Molecular cloning of cDNA encoding the Ca2+ release channel (ryanodine receptor) of rabbit cardiac muscle sarcoplasmic reticulum. *J. Biol. Chem.* **265**, 13472–13483 (1990).

14. Nakashima, Y. *et al.* Molecular cloning and characterization of a human brain ryanodine receptor 1. *FEBS Lett.* **417**, 157–162 (1997).

15. Takeshima, H. *et al.* Primary structure and expression from complementary DNA of skeletal muscle ryanodine receptor. *Nature* **339**, 439–445 (1989).

16. Jayasinghe, I. *et al.* True Molecular Scale Visualization of Variable Clustering Properties of Ryanodine Receptors. *Cell Rep.* **22**, 557–567 (2018).

17. Soeller, C., Crossman, D., Gilbert, R. & Cannell, M. B. Analysis of ryanodine receptor clusters in rat and human cardiac myocytes. *Proc. Natl. Acad. Sci. U. S. A.* **104**, 14958–14963 (2007).

18. Franzini-Armstrong, C., Protasi, F. & Ramesh, V. Shape, size, and distribution of Ca(2+) release units and couplons in skeletal and cardiac muscles. *Biophys. J.* **77**, 1528–1539 (1999).

19. Zhao, M. *et al.* Molecular identification of the ryanodine receptor pore-forming segment. *J. Biol. Chem.* **274**, 25971–25974 (1999).

20. Anderson, K. *et al.* Structural and functional characterization of the purified cardiac ryanodine receptor-Ca2+ release channel complex. *J. Biol. Chem.* **264**, 1329–1335 (1989).

21. Wehrens, X. H. T. *et al.* Ryanodine receptor/calcium release channel PKA phosphorylation: A critical mediator of heart failure progression. *Proc. Natl. Acad. Sci.* **103**, 511–518 (2006).

22. Wehrens, X. H. T., Lehnart, S. E., Reiken, S. R. & Marks, A. R. Ca2+/calmodulin-dependent protein kinase II phosphorylation regulates the cardiac ryanodine receptor. *Circ. Res.* **94**, e61-70 (2004).

23. Kushnir, A., Wajsberg, B. & Marks, A. R. Ryanodine receptor dysfunction in human disorders. *Biochim. Biophys. Acta BBA - Mol. Cell Res.* **1865**, 1687–1697 (2018).

24. Marx, S. O. *et al.* Phosphorylation-dependent regulation of ryanodine receptors: a novel role for leucine/isoleucine zippers. *J. Cell Biol.* **153**, 699–708 (2001).

25. Timerman, A. P. *et al.* Selective binding of FKBP12.6 by the cardiac ryanodine receptor. *J. Biol. Chem.* **271**, 20385–20391 (1996).

26. Bers, D. M. Macromolecular complexes regulating cardiac ryanodine receptor function. *J. Mol. Cell. Cardiol.* **37**, 417–429 (2004).

27. Wehrens, X. H. T. *et al.* FKBP12.6 deficiency and defective calcium release channel (ryanodine receptor) function linked to exercise-induced sudden cardiac death. *Cell* **113**, 829–840 (2003).

28. Lehnart, S. E. *et al.* Sudden death in familial polymorphic ventricular tachycardia associated with calcium release channel (ryanodine receptor) leak. *Circulation* **109**, 3208–3214 (2004).

29. *Electrical Diseases of the Heart: Volume 2: Diagnosis and Treatment*. (Springer-Verlag, 2013). doi:10.1007/978-1-4471-4978-1.

30. Tripathy, A., Xu, L., Mann, G. & Meissner, G. Calmodulin activation and inhibition of skeletal muscle Ca2+ release channel (ryanodine receptor). *Biophys. J.* **69**, 106–119 (1995).

31. Moore, C. P. *et al.* Apocalmodulin and Ca2+ calmodulin bind to the same region on the skeletal muscle Ca2+ release channel. *Biochemistry* **38**, 8532–8537 (1999).

32. Xu, X. *et al.* Defective calmodulin binding to the cardiac ryanodine receptor plays a key role in CPVT-associated channel dysfunction. *Biochem. Biophys. Res. Commun.* **394**, 660–666 (2010).

33. Rossi, D. *et al.* Calsequestrin, a key protein in striated muscle health and disease. *J. Muscle Res. Cell Motil.* **42**, 267–279 (2021).

34. Zhang, L., Kelley, J., Schmeisser, G., Kobayashi, Y. M. & Jones, L. R. Complex Formation between Junctin, Triadin, Calsequestrin, and the Ryanodine Receptor: PROTEINS OF THE

CARDIAC JUNCTIONAL SARCOPLASMIC RETICULUM MEMBRANE *. *J. Biol. Chem.* **272**, 23389–23397 (1997).

35. Eager, K. R. & Dulhunty, A. F. Activation of the cardiac ryanodine receptor by sulfhydryl oxidation is modified by Mg2+ and ATP. *J. Membr. Biol.* **163**, 9–18 (1998).

36. Zable, A. C., Favero, T. G. & Abramson, J. J. Glutathione modulates ryanodine receptor from skeletal muscle sarcoplasmic reticulum. Evidence for redox regulation of the Ca2+ release mechanism. *J. Biol. Chem.* **272**, 7069–7077 (1997).

37. Xu, L., Eu, J. P., Meissner, G. & Stamler, J. S. Activation of the cardiac calcium release channel (ryanodine receptor) by poly-S-nitrosylation. *Science* **279**, 234–237 (1998).

38. Jones, D. P. Redefining oxidative stress. *Antioxid. Redox Signal.* **8**, 1865–1879 (2006).

39. Ghezzi, P., Bonetto, V. & Fratelli, M. Thiol-disulfide balance: from the concept of oxidative stress to that of redox regulation. *Antioxid. Redox Signal.* **7**, 964–972 (2005).

40. Poole, L. B. Formation and functions of protein sulfenic acids. *Curr. Protoc. Toxicol. Editor. Board Mahin Maines Ed.--Chief Al* **Chapter 17**, Unit17.1 (2004).

41. Gellert, M., Hanschmann, E.-M., Lepka, K., Berndt, C. & Lillig, C. H. Redox regulation of cytoskeletal dynamics during differentiation and de-differentiation. *Biochim. Biophys. Acta BBA - Gen. Subj.* **1850**, 1575–1587 (2015).

42. Gallogly, M. M. & Mieyal, J. J. Mechanisms of reversible protein glutathionylation in redox signaling and oxidative stress. *Curr. Opin. Pharmacol.* **7**, 381–391 (2007).

43. Hanschmann, E.-M., Godoy, J. R., Berndt, C., Hudemann, C. & Lillig, C. H. Thioredoxins, glutaredoxins, and peroxiredoxins--molecular mechanisms and health significance: from cofactors to antioxidants to redox signaling. *Antioxid. Redox Signal.* **19**, 1539–1605 (2013).

44. Forman, H. J., Fukuto, J. M. & Torres, M. Redox signaling: thiol chemistry defines which reactive oxygen and nitrogen species can act as second messengers. *Am. J. Physiol. Cell Physiol.* **287**, C246-256 (2004).

45. Krekel, F., Samland, A. K., Macheroux, P., Amrhein, N. & Evans, J. N. Determination of the pKa value of C115 in MurA (UDP-N-acetylglucosamine enolpyruvyltransferase) from Enterobacter cloacae. *Biochemistry* **39**, 12671–12677 (2000).

46. Deponte, M. & Lillig, C. H. Enzymatic control of cysteinyl thiol switches in proteins. *Biol. Chem.* **396**, 401–413 (2015).

47. Sies, H. Role of metabolic H2O2 generation: redox signaling and oxidative stress. *J. Biol. Chem.* **289**, 8735–8741 (2014).

48. Ullrich, V. & Kissner, R. Redox signaling: bioinorganic chemistry at its best. *J. Inorg. Biochem.* **100**, 2079–2086 (2006).

49. McCord, J. M. & Fridovich, I. Superoxide Dismutase AN ENZYMIC FUNCTION FOR ERYTHROCUPREIN (HEMOCUPREIN). *J. Biol. Chem.* **244**, 6049–6055 (1969).

50. Brand, M. D. The sites and topology of mitochondrial superoxide production. *Exp. Gerontol.* **45**, 466–472 (2010).

51. Lambeth, J. D. NOX enzymes and the biology of reactive oxygen. *Nat. Rev. Immunol.* **4**, 181–189 (2004).

52. Muller, F. L., Liu, Y. & Remmen, H. V. Complex III Releases Superoxide to Both Sides of the Inner Mitochondrial Membrane. *J. Biol. Chem.* **279**, 49064–49073 (2004).

53. Joubert, J. & Malan, S. F. Novel nitric oxide synthase inhibitors: a patent review. *Expert Opin. Ther. Pat.* **21**, 537–560 (2011).

54. Umar, S. & van der Laarse, A. Nitric oxide and nitric oxide synthase isoforms in the normal, hypertrophic, and failing heart. *Mol. Cell. Biochem.* **333**, 191–201 (2010).

55. Sies, H. Oxidative stress: from basic research to clinical application. *Am. J. Med.* **91**, 31S-38S (1991).

56. Ahsan, M. K., Lekli, I., Ray, D., Yodoi, J. & Das, D. K. Redox regulation of cell survival by the thioredoxin superfamily: an implication of redox gene therapy in the heart. *Antioxid. Redox Signal.* **11**, 2741–2758 (2009).

57. Lillig, C. H. & Holmgren, A. Thioredoxin and related molecules--from biology to health and disease. *Antioxid. Redox Signal.* **9**, 25–47 (2007).

58. Lillig, C. H., Berndt, C. & Holmgren, A. Glutaredoxin systems. *Biochim. Biophys. Acta BBA - Gen. Subj.* **1780**, 1304–1317 (2008).

59. Rhee, S. G., Kang, S. W., Chang, T. S., Jeong, W. & Kim, K. Peroxiredoxin, a novel family of peroxidases. *IUBMB Life* **52**, 35–41 (2001).

60. RYR2 - Ryanodine receptor 2 - Homo sapiens (Human) - RYR2 gene & protein. https://www.uniprot.org/uniprot/Q92736#sequences.

61. Voss, A. A., Lango, J., Ernst-Russell, M., Morin, D. & Pessah, I. N. Identification of hyperreactive cysteines within ryanodine receptor type 1 by mass spectrometry. *J. Biol. Chem.* **279**, 34514–34520 (2004).

62. Aracena-Parks, P. *et al.* Identification of Cysteines Involved in S-Nitrosylation, S-Glutathionylation, and Oxidation to Disulfides in Ryanodine Receptor Type 1 *. *J. Biol. Chem.* **281**, 40354–40368 (2006).

63. Donoso, P., Sanchez, G., Bull, R. & Hidalgo, C. Modulation of cardiac ryanodine receptor activity by ROS and RNS. *Front. Biosci. Landmark Ed.* **16**, 553–567 (2011).

64. Gonzalez, D. R., Treuer, A., Sun, Q.-A., Stamler, J. S. & Hare, J. M. S-nitrosylation of cardiac ion channels. *J. Cardiovasc. Pharmacol.* **54**, 188–195 (2009).

65. Mészáros, L. G., Minarovic, I. & Zahradnikova, A. Inhibition of the skeletal muscle ryanodine receptor calcium release channel by nitric oxide. *FEBS Lett.* **380**, 49–52 (1996).

66. Gonzalez, D. R., Treuer, A. V., Castellanos, J., Dulce, R. A. & Hare, J. M. Impaired S-nitrosylation of the ryanodine receptor caused by xanthine oxidase activity contributes to calcium leak in heart failure. *J. Biol. Chem.* **285**, 28938–28945 (2010).

67. Sun, J. & Murphy, E. Protein S-nitrosylation and cardioprotection. *Circ. Res.* **106**, 285–296 (2010).

68. Townsend, D. M. S-glutathionylation: indicator of cell stress and regulator of the unfolded protein response. *Mol. Interv.* **7**, 313–324 (2007).

69. Sánchez, G. *et al.* Exercise and tachycardia increase NADPH oxidase and ryanodine receptor-2 activity: possible role in cardioprotection. *Cardiovasc. Res.* **77**, 380–386 (2008).

70. Brennan, J. P. *et al.* Detection and mapping of widespread intermolecular protein disulfide formation during cardiac oxidative stress using proteomics with diagonal electrophoresis. *J. Biol. Chem.* **279**, 41352–41360 (2004).

71. Terentyev, D. *et al.* Redox Modification of Ryanodine Receptors Contributes to Sarcoplasmic Reticulum Ca2+ Leak in Chronic Heart Failure. *Circ. Res.* **103**, 1466–1472 (2008).

72. Bedard, K. & Krause, K.-H. The NOX Family of ROS-Generating NADPH Oxidases: Physiology and Pathophysiology. *Physiol. Rev.* **87**, 245–313 (2007).

73. Rossi, F. & Zatti, M. Biochemical aspects of phagocytosis in poly-morphonuclear leucocytes. NADH and NADPH oxidation by the granules of resting and phagocytizing cells. *Experientia* **20**, 21–23 (1964).

74. Finegold, A. A., Shatwell, K. P., Segal, A. W., Klausner, R. D. & Dancis, A. Intramembrane Bis-Heme Motif for Transmembrane Electron Transport Conserved in a Yeast Iron Reductase and the Human NADPH Oxidase *. *J. Biol. Chem.* **271**, 31021–31024 (1996).

75. Segal, A. W. *et al.* Cytochrome b-245 is a flavocytochrome containing FAD and the NADPH-binding site of the microbicidal oxidase of phagocytes. *Biochem. J.* **284**, 781–788 (1992).

76. Cross, A. R. & Segal, A. W. The NADPH oxidase of professional phagocytes—prototype of the NOX electron transport chain systems. *Biochim. Biophys. Acta BBA - Bioenerg.* **1657**, 1–22 (2004).

77. GROEMPING, Y. & RITTINGER, K. Activation and assembly of the NADPH oxidase: a structural perspective. *Biochem. J.* **386**, 401–416 (2005).

78. Dinauer, M. C., Pierce, E. A., Bruns, G. A., Curnutte, J. T. & Orkin, S. H. Human neutrophil cytochrome b light chain (p22-phox). Gene structure, chromosomal location, and mutations in cytochrome-negative autosomal recessive chronic granulomatous disease. *J. Clin. Invest.* **86**, 1729–1737 (1990).

79. Groemping, Y., Lapouge, K., Smerdon, S. J. & Rittinger, K. Molecular Basis of Phosphorylation-Induced Activation of the NADPH Oxidase. *Cell* **113**, 343–355 (2003).

80. Schröder, K., Weissmann, N. & Brandes, R. P. Organizers and activators: Cytosolic Nox proteins impacting on vascular function. *Free Radic. Biol. Med.* **109**, 22–32 (2017).

81. Diebold, B. A. & Bokoch, G. M. Molecular basis for Rac2 regulation of phagocyte NADPH oxidase. *Nat. Immunol.* **2**, 211–215 (2001).

82. Lapouge, K. *et al.* Structure of the TPR Domain of p67phox in Complex with Rac·GTP. *Mol. Cell* **6**, 899–907 (2000).

83. Suh, Y.-A. *et al.* Cell transformation by the superoxide-generating oxidase Mox1. *Nature* **401**, 79–82 (1999).

84. Bánfi, B. *et al.* NOX3, a Superoxide-generating NADPH Oxidase of the Inner Ear *. *J. Biol. Chem.* **279**, 46065–46072 (2004).

85. Szanto, I. *et al.* Expression of NOX1, a superoxide-generating NADPH oxidase, in colon cancer and inflammatory bowel disease. *J. Pathol.* **207**, 164–176 (2005).

86. Lassègue, B. *et al.* Novel gp91phox Homologues in Vascular Smooth Muscle Cells. *Circ. Res.* **88**, 888–894 (2001).

87. Ago, T. *et al.* NAD(P)H Oxidases in Rat Basilar Arterial Endothelial Cells. *Stroke* **36**, 1040–1046 (2005).

88. Vermot, A., Petit-Härtlein, I., Smith, S. M. E. & Fieschi, F. NADPH Oxidases (NOX): An Overview from Discovery, Molecular Mechanisms to Physiology and Pathology. *Antioxidants* **10**, 890 (2021).

89. Takeya, R. *et al.* Novel human homologues of p47phox and p67phox participate in activation of superoxide-producing NADPH oxidases. *J. Biol. Chem.* **278**, 25234–25246 (2003).

90. Cheng, G., Ritsick, D. & Lambeth, J. D. Nox3 regulation by NOXO1, p47phox, and p67phox. *J. Biol. Chem.* **279**, 34250–34255 (2004).

91. Geiszt, M., Kopp, J. B., Várnai, P. & Leto, T. L. Identification of Renox, an NAD(P)H oxidase in kidney. *Proc. Natl. Acad. Sci.* **97**, 8010–8014 (2000).

92. Goyal, P. *et al.* Identification of novel Nox4 splice variants with impact on ROS levels in A549 cells. *Biochem. Biophys. Res. Commun.* **329**, 32–39 (2005).

93. Martyn, K. D., Frederick, L. M., von Loehneysen, K., Dinauer, M. C. & Knaus, U. G. Functional analysis of Nox4 reveals unique characteristics compared to other NADPH oxidases. *Cell. Signal.* **18**, 69–82 (2006).

94. Kawahara, T., Ritsick, D., Cheng, G. & Lambeth, J. D. Point Mutations in the Proline-rich Region of p22phox Are Dominant Inhibitors of Nox1- and Nox2-dependent Reactive Oxygen Generation *. *J. Biol. Chem.* **280**, 31859–31869 (2005).

95. Gray, S. P., Shah, A. M. & Smyrnias, I. NADPH oxidase 4 and its role in the cardiovascular system. *Vasc. Biol. Bristol Engl.* **1**, H59–H66 (2019).

96. Takac, I. *et al.* The E-loop Is Involved in Hydrogen Peroxide Formation by the NADPH Oxidase Nox4. *J. Biol. Chem.* **286**, 13304–13313 (2011).

97. Bánfi, B. *et al.* A Ca2+-activated NADPH Oxidase in Testis, Spleen, and Lymph Nodes *. *J. Biol. Chem.* **276**, 37594–37601 (2001).

98. Deken, X. D. *et al.* Cloning of Two Human Thyroid cDNAs Encoding New Members of the NADPH Oxidase Family *. *J. Biol. Chem.* **275**, 23227–23233 (2000).

99. Ameziane-El-Hassani, R. *et al.* Dual Oxidase-2 Has an Intrinsic Ca2+-dependent H2O2-generating Activity *. *J. Biol. Chem.* **280**, 30046–30054 (2005).

100. Li, J.-M., Gall, N. P., Grieve, D. J., Chen, M. & Shah, A. M. Activation of NADPH oxidase during progression of cardiac hypertrophy to failure. *Hypertens. Dallas Tex 1979* **40**, 477–484 (2002).

101. Byrne, *, Jonathan A. *et al.* Contrasting Roles of NADPH Oxidase Isoforms in Pressure-Overload Versus Angiotensin II–Induced Cardiac Hypertrophy. *Circ. Res.* **93**, 802–805 (2003).

102. Heymes, C. *et al.* Increased myocardial NADPH oxidase activity in human heart failure. *J. Am. Coll. Cardiol.* **41**, 2164–2171 (2003).

103. Akki, A., Zhang, M., Murdoch, C., Brewer, A. & Shah, A. M. NADPH oxidase signaling and cardiac myocyte function. *J. Mol. Cell. Cardiol.* **47**, 15–22 (2009).

104. Faust, L. R., el Benna, J., Babior, B. M. & Chanock, S. J. The phosphorylation targets of p47phox, a subunit of the respiratory burst oxidase. Functions of the individual target serines as evaluated by site-directed mutagenesis. *J. Clin. Invest.* **96**, 1499–1505 (1995).

105. Prior, K.-K. *et al.* The Endoplasmic Reticulum Chaperone Calnexin Is a NADPH Oxidase NOX4 Interacting Protein. *J. Biol. Chem.* **291**, 7045–7059 (2016).

106. Anilkumar, N. *et al.* A 28-kDa splice variant of NADPH oxidase-4 is nuclear-localized and involved in redox signaling in vascular cells. *Arterioscler. Thromb. Vasc. Biol.* **33**, e104-112 (2013).

107. Satoh, M. *et al.* Requirement of Rac1 in the development of cardiac hypertrophy. *Proc. Natl. Acad. Sci. U. S. A.* **103**, 7432–7437 (2006).

108. Prosser, B. L., Khairallah, R. J., Ziman, A. P., Ward, C. W. & Lederer, W. J. X-ROS signaling in heart and skeletal muscle: stretch-dependent local ROS regulates [Ca2+]i. *J. Mol. Cell. Cardiol.* **58**, 172–181 (2013).

109. Zhang, M. *et al.* NADPH oxidase-4 mediates protection against chronic load-induced stress in mouse hearts by enhancing angiogenesis. *Proc. Natl. Acad. Sci.* **107**, 18121–18126 (2010).

110. Sun, Q.-A. *et al.* Oxygen-coupled redox regulation of the skeletal muscle ryanodine receptor-Ca2+ release channel by NADPH oxidase 4. *Proc. Natl. Acad. Sci. U. S. A.* **108**, 16098–16103 (2011).

111. Wagner, E., Brandenburg, S., Kohl, T. & Lehnart, S. E. Analysis of tubular membrane networks in cardiac myocytes from atria and ventricles. *J. Vis. Exp. JoVE* e51823 (2014) doi:10.3791/51823.

112. Janssen, P. M. L. *et al.* The trabecula culture system: a novel technique to study contractile parameters over a multiday time period. *Am. J. Physiol.-Heart Circ. Physiol.* **274**, H1481–H1488 (1998).

113. Wagner, E. *et al.* Stimulated Emission Depletion Live-Cell Super-Resolution Imaging Shows Proliferative Remodeling of T-Tubule Membrane Structures After Myocardial Infarction. *Circ. Res.* **111**, 402–414 (2012).

114. Campbell, H. M. *et al.* Loss of SPEG Inhibitory Phosphorylation of Ryanodine Receptor Type-2 Promotes Atrial Fibrillation. *Circulation* **142**, 1159–1172 (2020).

115. Anilkumar, N., Weber, R., Zhang, M., Brewer, A. & Shah, A. M. Nox4 and Nox2 NADPH Oxidases Mediate Distinct Cellular Redox Signaling Responses to Agonist Stimulation. *Arterioscler. Thromb. Vasc. Biol.* **28**, 1347–1354 (2008).

116. Kleinschnitz, C. *et al.* Post-Stroke Inhibition of Induced NADPH Oxidase Type 4 Prevents Oxidative Stress and Neurodegeneration. *PLOS Biol.* **8**, e1000479 (2010).

117. Nox4 - NADPH oxidase 4 - Mus musculus (Mouse) - Nox4 gene & protein. https://www.uniprot.org/uniprot/Q9JHI8#sequences.

118. Munro, M. L. *et al.* Junctophilin-2 in the nanoscale organisation and functional signalling of ryanodine receptor clusters in cardiomyocytes. *J. Cell Sci.* **129**, 4388–4398 (2016).

119. Anjo, S. I. *et al.* oxSWATH: An integrative method for a comprehensive redox-centered analysis combined with a generic differential proteomics screening. *Redox Biol.* **22**, 101130 (2019).

120. Zhao, F., Li, P., Chen, S. R. W., Louis, C. F. & Fruen, B. R. Dantrolene Inhibition of Ryanodine Receptor Ca2+Release Channels: MOLECULAR MECHANISM AND ISOFORM SELECTIVITY *. *J. Biol. Chem.* **276**, 13810–13816 (2001).

121. Gao, L., Tripathy, A., Lu, X. & Meissner, G. Evidence for a role of C-terminal amino acid residues in skeletal muscle Ca2+ release channel (ryanodine receptor) function. *FEBS Lett.* **412**, 223–226 (1997).

122. Meissner, G. Ryanodine activation and inhibition of the Ca2+ release channel of sarcoplasmic reticulum. *J. Biol. Chem.* **261**, 6300–6306 (1986).

123. Waddell, H. M. M. *et al.* Oxidation of RyR2 Has a Biphasic Effect on the Threshold for Store Overload-Induced Calcium Release. *Biophys. J.* **110**, 2386–2396 (2016).

124. Federico, M., Valverde, C. A., Mattiazzi, A. & Palomeque, J. Unbalance Between Sarcoplasmic Reticulum Ca2 + Uptake and Release: A First Step Toward Ca2 + Triggered Arrhythmias and Cardiac Damage. *Front. Physiol.* **10**, 1630 (2020).

125. Jones, P. P., MacQuaide, N. & Louch, W. E. Dyadic Plasticity in Cardiomyocytes. *Front. Physiol.* **9**, 1773 (2018).

126. Sandoval, R. *et al.* TNF-α Increases Production of Reactive Oxygen Species through Cdk5 Activation in Nociceptive Neurons. *Front. Physiol.* **9**, 65 (2018).

127. Reis, J. *et al.* A closer look into NADPH oxidase inhibitors: Validation and insight into their mechanism of action. *Redox Biol.* **32**, 101466 (2020).

128. Limbu, S., Prosser, B. L., Lederer, W. J., Ward, C. W. & Jafri, M. S. X-ROS Signaling Depends on Length-Dependent Calcium Buffering by Troponin. *Cells* **10**, 1189 (2021).

129. Palmer, A. E., Jin, C., Reed, J. C. & Tsien, R. Y. Bcl-2-mediated alterations in endoplasmic reticulum Ca2+ analyzed with an improved genetically encoded fluorescent sensor. *Proc. Natl. Acad. Sci. U. S. A.* **101**, 17404–17409 (2004).

130. Suzuki, J., Kanemaru, K. & Iino, M. Genetically Encoded Fluorescent Indicators for Organellar Calcium Imaging. *Biophys. J.* **111**, 1119–1131 (2016).

131. Block, K., Gorin, Y. & Abboud, H. E. Subcellular localization of Nox4 and regulation in diabetes. *Proc. Natl. Acad. Sci. U. S. A.* **106**, 14385–14390 (2009).

132. Bernhem, K., Blom, H. & Brismar, H. Quantification of endogenous and exogenous protein expressions of Na,K-ATPase with super-resolution PALM/STORM imaging. *PLOS ONE* **13**, e0195825 (2018).

133. Gibson, T. J., Seiler, M. & Veitia, R. A. The transience of transient overexpression. *Nat. Methods* **10**, 715–721 (2013).

134. O'Connell, T. D., Rodrigo, M. C. & Simpson, P. C. Isolation and culture of adult mouse cardiac myocytes. *Methods Mol. Biol. Clifton NJ* **357**, 271–296 (2007).

135. Brandenburg, S. *et al.* Axial tubule junctions control rapid calcium signaling in atria. *J. Clin. Invest.* **126**, 3999–4015.

136. Dridi, H. *et al.* Role of defective calcium regulation in cardiorespiratory dysfunction in Huntington's disease. *JCI Insight* **5**, e140614.

137. Santos, C. X. C., Anilkumar, N., Zhang, M., Brewer, A. C. & Shah, A. M. Redox signaling in cardiac myocytes. *Free Radic. Biol. Med.* **50**, 777–793 (2011).

138. Burgoyne, J. R., Mongue-Din, H., Eaton, P. & Shah, A. M. Redox Signaling in Cardiac Physiology and Pathology. *Circ. Res.* **111**, 1091–1106 (2012).

139. Nakagami, H., Takemoto, M. & Liao, J. K. NADPH oxidase-derived superoxide anion mediates angiotensin II-induced cardiac hypertrophy. *J. Mol. Cell. Cardiol.* **35**, 851–859 (2003).

140. Xiao, L. *et al.* Role of reactive oxygen species and NAD(P)H oxidase in alpha(1)-adrenoceptor signaling in adult rat cardiac myocytes. *Am. J. Physiol. Cell Physiol.* **282**, C926-934 (2002).

141. Kuster, G. M. *et al.* Alpha-adrenergic receptor-stimulated hypertrophy in adult rat ventricular myocytes is mediated via thioredoxin-1-sensitive oxidative modification of thiols on Ras. *Circulation* **111**, 1192–1198 (2005).

142. Bendall, J. K., Cave, A. C., Heymes, C., Gall, N. & Shah, A. M. Pivotal role of a gp91(phox)-containing NADPH oxidase in angiotensin II-induced cardiac hypertrophy in mice. *Circulation* **105**, 293–296 (2002).

143. Swain, L. *et al.* Redox Imaging Using Cardiac Myocyte-Specific Transgenic Biosensor Mice. *Circ. Res.* **119**, 1004–1016 (2016).

# Appendix

## A

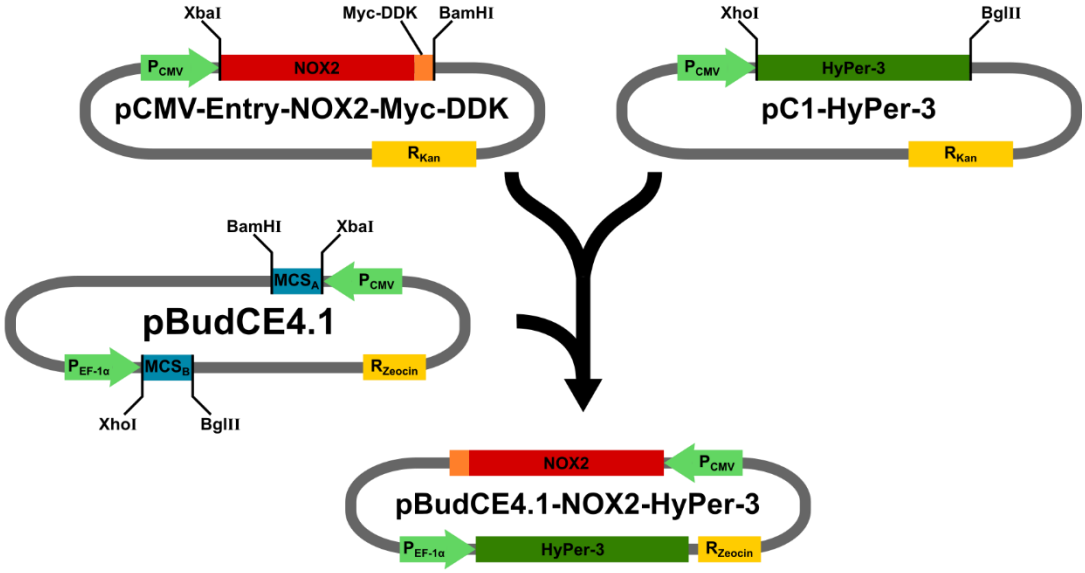


## B

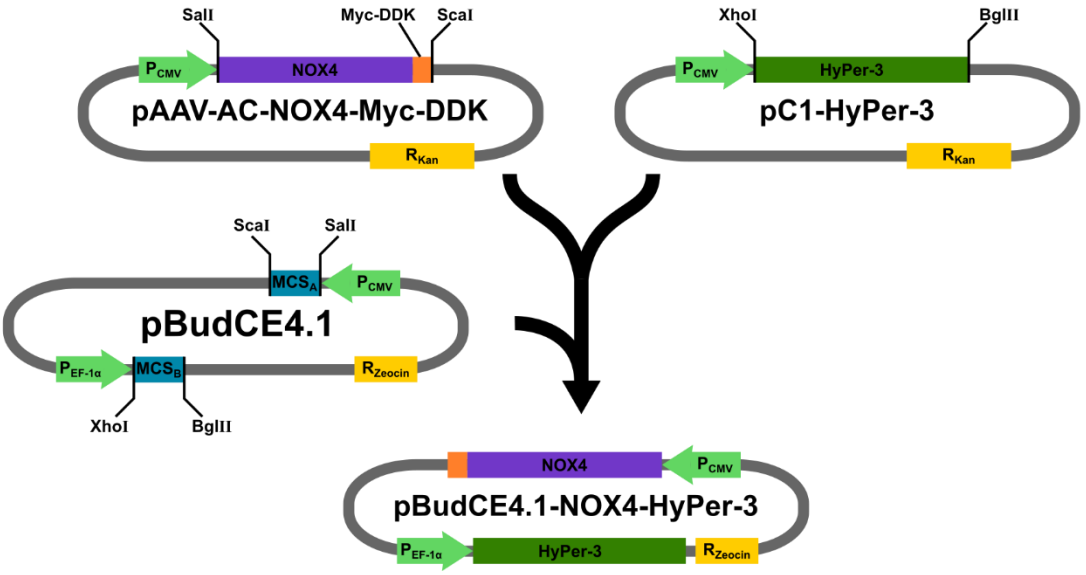


***Figure 20: Cloning scheme for the generation of pBudCE4.1-NOX2-HyPer-3 and pBudCE4.1-NOX4-HyPer3 expression vectors.***

*Both NOX2* ***(A)*** *and NOX4* ***(B)*** *as well as HyPer-3 were excised from their original vector backbone using the indicated restriction enzymes. NOX2 and HyPer-3 or NOX4 and HyPer-3, respectively, were combined into the pBudCE4.1 vector backbone.*

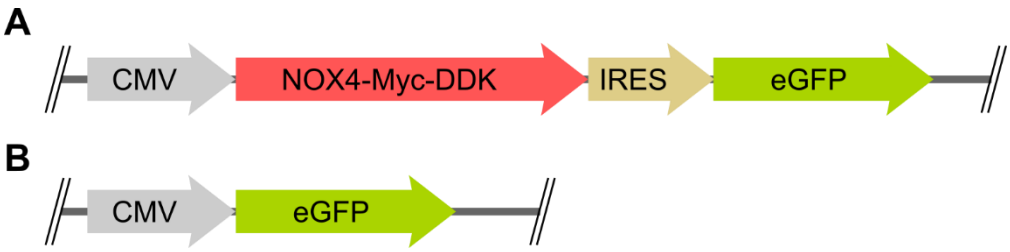


***Figure 21: Adenoviral constructs for transduction of isolated ventricular cardiomyocytes.***

*Adenoviral particles, serotype 5 (Ad5) were used to introduce a CMV-driven constitutive NOX4 expression* ***(A)*** *or eGFP as a control* ***(B)*** *in isolated myocytes. For the NOX4 expression construct, eGFP was additionally used as a transfection control.*

# Curriculum Vitae